UNIVERSITÀ DEGLI STUDI DI PADOVA

UNIVERSITA' DEGLI STUDI DI PADOVA

Dipartimento di Ingegneria Industriale DII

Corso di Laurea Magistrale in Ingegneria dell'Energia Elettrica

Design Methodology and Simulation of a Nine-Phase Induction Machine for a Test Bench

Relatore : Prof. Nicola Bianchi

Correlatori : Univ.-Prof. Dr.-Ing. Hans-Georg Herzog

Dipl.-Ing. Jörg Kammermann

Federico Pomari 1137586

Anno Accademico 2018/2019

Abstract

The growth of interest in the field of the electrical transportation requires high level of reliability and fault tolerance. Alternative solutions to the classical three-phase machine are investigate in scientific literature in order to satisfy these characteristics. It has been seen that multi-phase machines are a good solution since they have several advantages: reduced power per phase,reduced rotor harmonics current, lower torque pulsation, higher reliability and power density. A good solution, in this sense, is to adopt a nine-phase machine and since permanent magnet machine are largely studied in the scientific literature, a nine-phase induction machine is consider. The aim of this thesis is to design an 11 kVA induction machine as an alternative to another permanent magnet machine with the same design specification, by proposing a general procedure. In the chapter 2 a distributed winding synthesis is addressed, by imposing the condition of feasibility. As the number of phase increases, become more difficult to build a distribute winding and therefore it is necessary a trade off between the desire magnetic proprieties and the mechanical feasibility. In 3 the design of the 11 kVA induction machine is proposed. Starting from the a certain utilization level of the machine, the size are obtained. Successively the stator and rotor geometry are designed taking into account of the unconventional phase system. In the chapters 4 and 5 an analytical and finite elements analysis of the designed machine are performed in order to have a verification on the machine. By the comparison of the two analysis the design is verified. The finite elements simulation is carried out with the combination of analytical 3D parameters and two-dimensional solution of the magnetic problem. Finally in chapter 6, after the verification of the finite elements results, the performance of the machine are calculated. In particular the machine respect the required specification of torque T =32 Nm and high efficiency $\eta = 88\%$.

Contents

List of Figures

List of Tables

1 Motivation of work

The increasing impact of pollution on the climatic balance has forced scientific research and industry towards an improvement of all technologies based on electricity as energy vector. Nowadays, a great contribution to the world pollution is given by the transport sector since it is based on fossil fuel for the most part. This is the reason why the attention to developing different solution with respect conventional mobility has grown in the last years. In particular designing even more efficient and more reliable electric machines is one of the tasks to achieve environmental sustainable widespread technologies in the sector of the transports. This include electric and hybrid vehicles, locomotive traction, electric ship propulsion and aerospace application [15]. Since nowadays AC drive can be supplied from power electronics very easily, the number of phase of the machines is not limited to three any more; in this sense, multi-phase machines could be a very interesting solutions because they can satisfy better the specification required from these applications. All type of multi-phase drive have common several advantages [15], [14]. [13]:

- The fault tolerant operation is the most important advantage and it is fundamental in the aerospace application. The redundancy of the phases allows to the machine to operate even with a phase-fault: a m-phase machine is able to operate with up (m-3) faulty phases, with an obvious drop in the produced torque. The most common failure case analyzed is the open-phase fault [5]
- For a given machine's output power, each phases is interested by a lower power. This this allows both to decrease the resistive losses and to adopt power electronics with lower current rating.

Figure 1.1 present a summary of the advantages with respect the three phase case. Focusing on machines with distributed stator winding additional advantage can be founded [14]:

- Lower torque ripple with respect the three-phase case: the frequency of the lowest ripple increases with m proportional to $2m$
- Lower harmonic content in the magneto-motive force (MMF) waveform $2m \pm 1$

Machine characterised by a concentrated windings have interesting features as well. The most important is the possibility to increase the torque density with the injection of higher order current harmonics, in order to couple all odd harmonics produced by the winding with a corresponding MMF harmonics of to produce torque [15].

Multi-phase permanent magnet machines (PM) with concentrated winding are largely studied in the scientific literature [22], [13], because they are very performing from the point of view of power and torque density. Nevertheless also the induction machine (IM) could be an attractive solution in the field of multi-phase drives. The IM are very rugged since there is no presence of PM in the machine and therefore there is no problems related to the demagnetization. Machines without PM could be also an economic advantage in the future

Property	Three-phase machine	Multiphase (n-phase) machine
Torque ripple frequency (f = fundamental frequency)	$6f$	$2nf$ ($> 6f$)
Order of the lowest spatial mmf harmonics (sinusoidal mmf machines)	5 and 7	$2n \pm 1$ ($> 5,7$)
Power/torque per phase (rated power/torque = P/T_e)	$P/3$ ($T_e/3$)	P/n (T_e/n)
Continued operation after an open-phase fault	No[1]	Yes[2]
Torque enhancement by stator current harmonic injection	Not possible	Yes (concentrated winding machines)

[1]Not possible without modification of the power converter topology.
[2]Requires derating after default for continuous post-fault operation.

Figure 1.1 – Overview of main advantages of multiphase machines [15]

because the majority of reserves of rare-earth magnet are in only few countries and this can cause strong fluctuations of the price. Finally the technology of construction of IM is mature and relatively easy, especially with regard the rotor that is build as cage for relatively low power of the transport sector.

2 Multi-phase distributed winding design for induction machine

A few concepts regarding the winding design of a multi-phase induction machine are presented. The whole design process requests aspects often contradicting each other and therefore is necessary to take all of them into account and find an acceptable trade-off that satisfies both the desirable performances of the machine and technical feasibility. The possible types of winding applied to IM and phases type connection are taking into account to ensure a general criteria of design for this unconventional machine. Finally, a winding scheme for the required machine is proposed,that it will be useful in the following chapter.

2.1 Analytical model of machine

At the beginning of the design process it is allowed to consider a simple model of the machine which it can be applied to any rotating machine, 2.1. For this discussion two reference systems

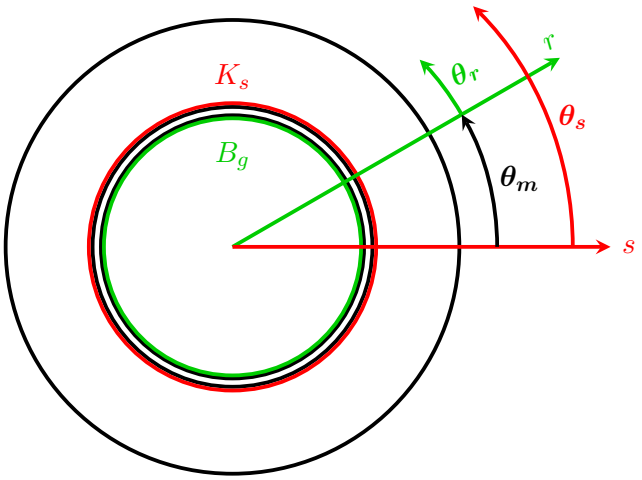

Figure 2.1 – Simplified model of rotating machine

are defined, one fixed to the rotor and the other one fixed to the stator. The rotor is the source of the flux density along the airgap, and its maximum value is along the polar axis r

$$B_g(\theta_r) = \hat{B}_g \cdot \cos(\theta_r) \tag{2.1}$$

Moreover it can be considered an infinitesimal conductor on the stator on which is distributed a linear current density K_s :

$$K_s(\theta_s) = \hat{K}_s \cdot \cos(\theta_s - \beta_s) \tag{2.2}$$

where by the definition:

$$\hat{K_s} = \frac{m \cdot k_w \cdot N_s \cdot \hat{I}}{2\pi \cdot D} \tag{2.3}$$

and β_s is the current phase angle referring to the s-axis. The interaction between $B_g(\theta_r)$ and $K_s(\theta_s)$ is under analysis and to do this the change of variables $\theta_s = \theta_r + \theta_m$ is carried out. Therefore the equation 2.1 is expressed in the stator system:

$$B_g(\theta_r) = \hat{B_g} \cdot \cos(\theta_s - \theta_m) \tag{2.4}$$

According the Lorentz's formula the infinitesimal force density in each position on the inner stator surface can be expressed as:

$$\begin{aligned} df(\theta_s) &= K_s(\theta_s) \cdot B_g(\theta_s) \\ &= \hat{K_s} \cdot \hat{B_g} \cdot \cos(\theta_s - \beta_s) \cdot \cos(\theta_s - \theta_m) \\ &= \frac{\hat{K_s} \cdot \hat{B_g}}{2} \cdot [\cos(2\theta_s - \beta_s - \theta_m) + (\beta_s - \theta_m)] \end{aligned} \tag{2.5}$$

by using trigonometrical relationships in the last step of 2.5. The total tangential force density along the whole periphery is calculate by :

$$F = \frac{1}{2\pi} \cdot \int_0^{2\pi} df(\theta_s)\, d(\theta_s) \tag{2.6}$$

If the equation 2.5 is taken into account then it can be noticed that the integral of the first term is zero because it varies with $2\theta_s$, instead the second term is constant, hence the equation 2.6 results:

$$F = \frac{\hat{K_s} \cdot \hat{B_g}}{2} \cos(\beta_s - \theta_m) \tag{2.7}$$

At this point it is possible to express the electromagnetic torque T_{em} acting on the rotor:

$$\begin{aligned} T_{em} &= F \cdot \pi \cdot D \cdot L \cdot \frac{D}{2} \\ &= \hat{K_s} \cdot \hat{B_g} \cdot \left(\frac{\pi}{4} \cdot D^2 \cdot L\right) \cdot \cos(\beta_s - \theta_m) \end{aligned} \tag{2.8}$$

The maximum value can be reached with $\beta_s = \theta_m$in other words when B_g and K_s are aligned.

$$T_{em} = \hat{K_s} \cdot \hat{B_g} \cdot \left(\frac{\pi}{4} \cdot D^2 \cdot L\right) \tag{2.9}$$

The electromagnetic torque is a important parameter for the beginning of the design: from the equation 2.9 it can been concluded that T_{em} is strictly related to the interaction between B_g and K_s and then, fixed the electrical and magnetic load, the torque is proportional to the

volume of the machine as well. Therefore the equation 2.9 can be used as starting point of the sizing of the machine.
The electric loading K_s is also the cause of the MMF distribution along the airgap according to:

$$U(\theta_s) = \int K(\theta_s) \cdot \frac{D}{2}\, d\theta \tag{2.10}$$

and the MMF distribution $U(\theta_s)$ has a maximum value

$$\hat{U} = \hat{K}_s \frac{D}{2p} \tag{2.11}$$

To the sinusoidal distribution of MMF corresponds to the sinusoidal flux density distribution presented before, given by:

$$\hat{B} = \mu_0 \frac{\hat{U}}{g''} \tag{2.12}$$

where g'' is the magnetic airgap thickness including Carter factor and saturation factor which will be described in the following chapters.

2.2 Choice of winding typology

The purpose is to design a symmetrical, multi-phase AC distributed slot winding, in other words rotating field winding. The first important issue to be addressed is the choice of the winding typology. Basically a multi-phase winding is described by q, the number of slot per pole and per phase, this quantity is characterised by a combination of the number of stator slot Q_s and the number of pole pair p :

$$q = \frac{Q_s}{2p \cdot m} \tag{2.13}$$

Depending on this quantity, the winding can be distributed if $q \geq 1$ (integer of factional slot according to whether $q \in \mathbb{Q}$ or $q \in \mathbb{N}$) or tooth-coil concentrated if $q < 1$. Each possible type has advantage and drawbacks.

According to the classical methodology [8], three-phase machines are usually designed with distributed winding in order to reach a near-sinusoidal MMF distribution and this aspect improves in the multiphase machines. Furthermore this type of solution presents large end windings, high parasitic end winding effects and high copper losses as in the case of three-phase machines [15]. By introducing the coil throw

$$y_q = \frac{Q_s}{2p} \tag{2.14}$$

and according the equation 2.13 the tooth - coil concentrated winding can be considered as a distributed winging with $y_q = 1$. This characteristic is the first advantage of this kind of solution related to manufacturing,indeed the teeth can be wound outside the machine and then inserted one after the other into the stator. In addition tooth - coil windings can theoretically produce higher torque than when using distributed windings dude to shorter end winding and therefore longer active length compared to distributed windings.

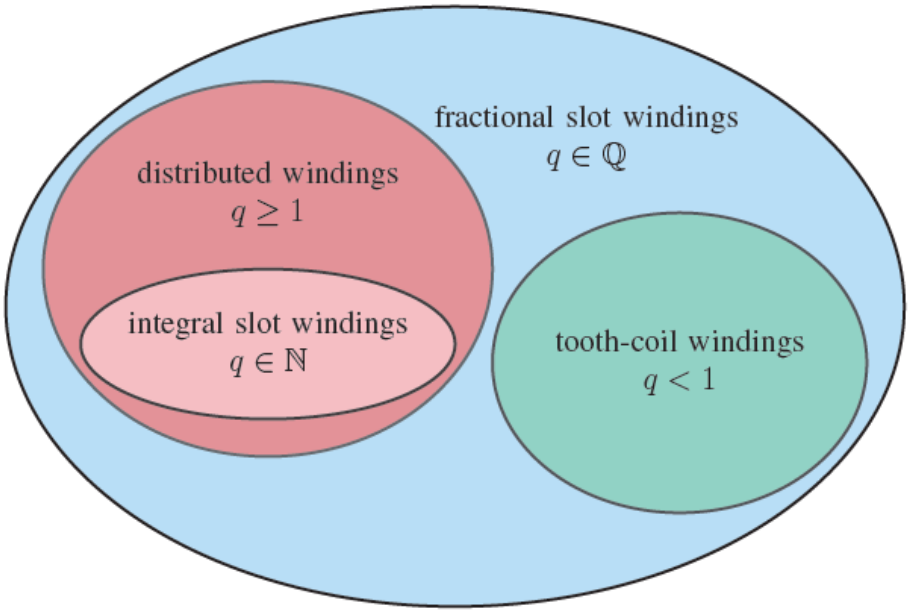

Figure 2.2 – Schematic representation all possible windings in relation to the number of slot per pole and per phase and their affiliated range of numbers [22]

Nevertheless tooth - coil concentrated winding has a big disadvantage in a very high number of space harmonics and also their amplitude, since the MMF produced at the airgap is quasi-rectangular. In the induction machines the electromagnetic torque is given only by the interaction between the stator and rotor fundamental field. The rotor reacts even with the space harmonics and this gives eddy torques overlapped on the main contribution called asynchronous torque [18]. This phenomenon causes additional rotor losses, torque ripple and acoustic noise during operation and consequently a decrease of efficiency; aspects to avoided in a machine for traction application. Nevertheless a tooth-coil machine does not necessarily work with the fundamental which the stator winding creates but with a harmonic which is called the operating harmonic [18], reference [19] concludes that traditional distributed winding is superior to concentrated winding in terms of torque production, rotor bar losses and tends to have higher torque ripple in the field of induction machines. Furthermore, the design of concentrated winding induction machine generally required a large number of poles that yields magnetization problems, and it is characterized by a high inductance which reduces the maximum torque [2]. A visual summary of all possible type of winding related to the number of slot per pole and per phase is reported in 2.2. After these considerations, the distributed winding is chosen as the best solution for the following design of the induction machine even though, considering multi-phase machines, since the number of phases increases with respect the three-phase case, it becomes difficult to realize a near-sinusoidal MMF distribution. This is because, more than one slot per pole and per phase q is required in order to reach the desired MMF distribution at the airgap [15]. Generally even a distributed fractional slot winding $q \geq 1 \ \cap \ q \in \mathbb{Q}$ can not be considered as a possible choice. This is because such solution can develop subharmonics in the MMF distribution which cause losses if the rotor has any conductivity, which is the case in induction machines [18] Nevertheless, under a specific condition even a distributed fractional slot winding is a possible solution.

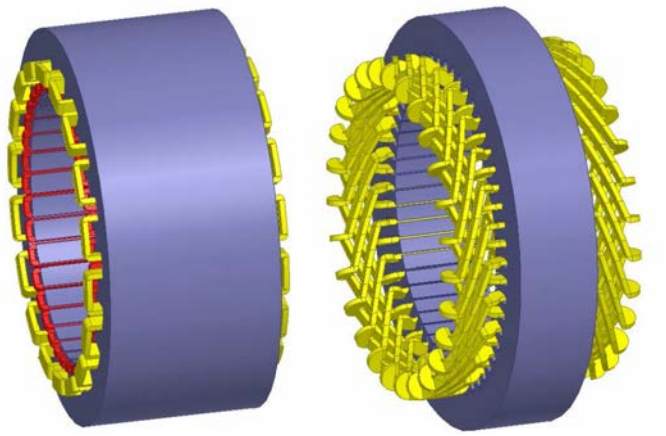

Figure 2.3 – Comparison of dimensions between IM and PM [10]

[9] in this case, shows that the slot-phase allocation repeats itself after each pole pair (for an integer q it repeats after each pole) therefore mmf subharmonics, or fractional space harmonics, are still absent in this case of fractional q. This property holds for

$$q = \frac{(2l+1)}{2} \tag{2.15}$$

for two-layer configurations, where $2l+1$ is coils-phase-pole pairs. A reduction of copper weight and an increase in efficiency may thus be obtained but there is the necessity of using nonidentical coils. Simplified 3D models of the two types of winding are compared in the figure 2.3.

2.3 Multi-phase systems connection

In the construction of a multi-phase system several type of connection are possible 2.4. On a magnetic axis, only one axis of a phase winding can be located. If another phase winding is located on the same axis, no true poly-phase system is obtained, because both windings produce parallel fluxes. Therefore, each phase system that involves an even number of phases is reduced to involving only half of the original number of phases. If the reduction produces a system with an odd number of phases, we obtain a radially symmetric poly-phase system, in other words a normal system. If the reduction produces a system with an even number of phases, the result is a reduced system [18]. So for a generic m-phase normal system, the electrical angle between two consecutive phases can be expressed as:

$$\alpha_{ph} = \frac{2\pi}{m \cdot p} \tag{2.16}$$

This is always the case if the number of phases is an odd prime number. However for a reduced system the displacement is :

$$\alpha_{ph} = \frac{\pi}{m \cdot p} \tag{2.17}$$

This is valid if the number of phases is even number or no-prime odd number. As mentioned above, this case is characterized by an asymmetrical distribution of the magnetic axes winding

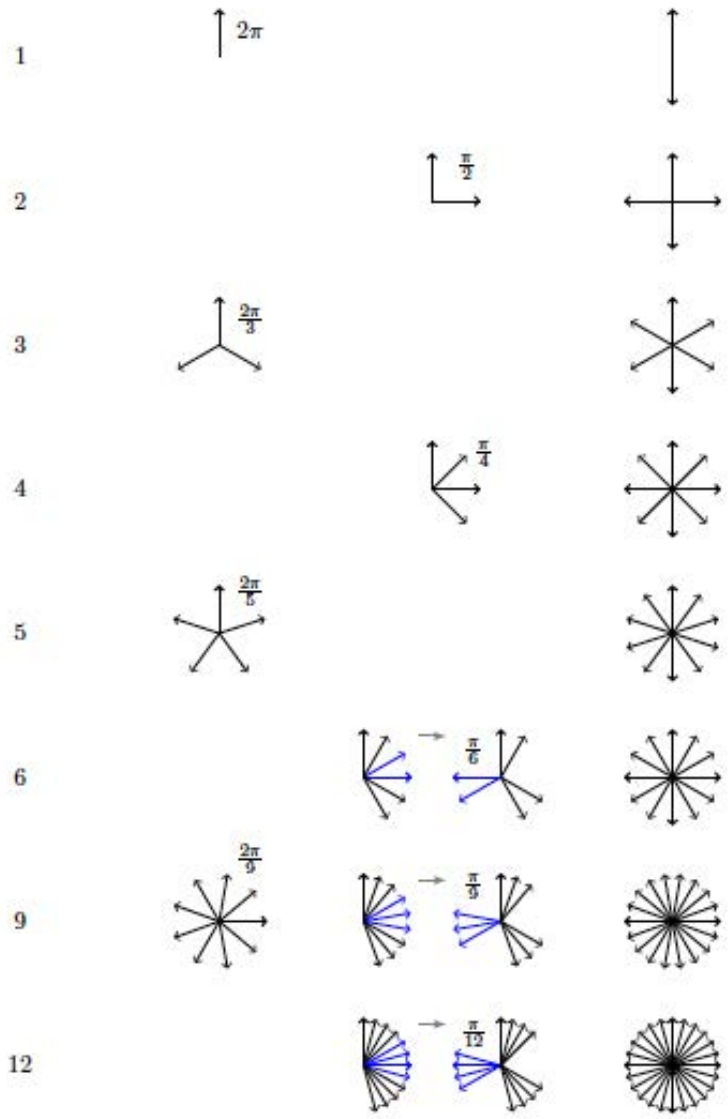

Figure 2.4 – Normal and reduced system for $m = 1,...,12$ [22]

because the winding can be realized as k windings having a sub-phases each, typical with $a = 3$ and $k = 2,3,4,5,...$ obtaining $m = a \cdot k$. In this configuration k neutral points are present and are generally kept isolated [15]. The dependence of MMF at the airgap, produced by the stator, on the phases connection is the the first important aspect to analyze. The case under analysis is $m = 9$ and therefore the possibilities regarding this configuration are investigated, bearing in mind that the machine will be supplied by inverter, the power electronics's configuration must be taken into account as well. The possible ways of connecting

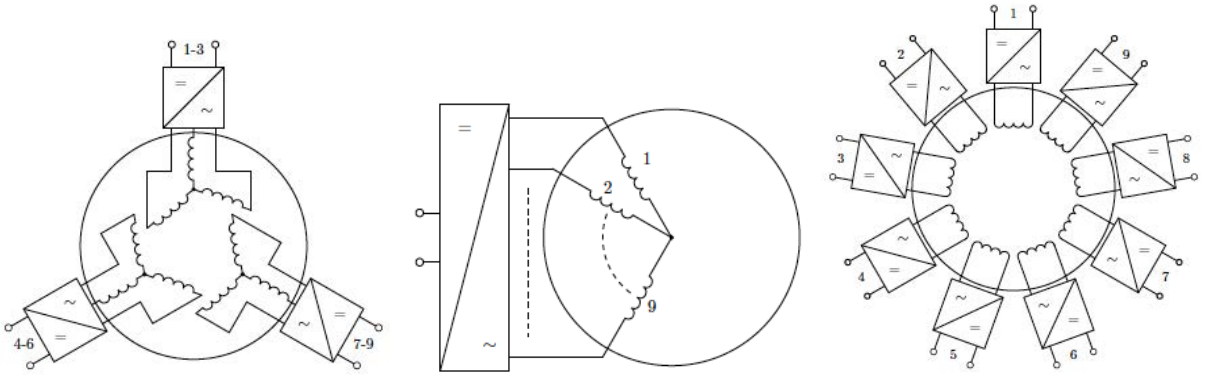

(a) *3x3-phase system with three star points* **(b)** *1x9-phase system with one star point* **(c)** *Nine galvanically separated phases*

Figure 2.5 – Possible ways of connecting power electronics [12]

.

power electronics and electrical machine are three and they are shown in 2.5 and the all their characteristics are discussed as well. In this particular case, by considering the characteristics of the test bench, only configurations 2.5a and 2.5b are available and therefore, on the basis of these two solution, the value of MMF is calculated.
According to the classical theory of electrical machines [4], since distributed winding has been chosen in 2.2,when it is fed by balanced system of AC currents, it produced rotating stepped MMF waveform composed of sum of all single phase fields:

$$U(\alpha,t) = \sum_{i=1}^{9} U_i(\alpha,t) \tag{2.18}$$

and

$$U_i(\alpha,t) = \hat{U}_i \ \sin(\omega \cdot t)\sin(\alpha) \tag{2.19}$$

where α is the electrical angular distance between two consecutive slots:

$$\alpha = \frac{x_c}{\tau}\ 2\pi \tag{2.20}$$

and x_c is the linear distance measured along the airgap. The equation 2.18 and 2.19 are written for the fundamental harmonic $\nu = 1$, but it is possible to extend the formula to higher order harmonics [2].

2.3.1 1x9-phase system

For normal systems with $m = 9$ and $p = 1$, from 2.13 the the angle between two consecutive phases is:

$$\begin{aligned} \alpha_{ph} &= \frac{2\pi}{m \cdot p} \\ &= \frac{2\pi}{9} = 40^\circ \end{aligned} \tag{2.21}$$

Since p is taken equal to 1 for for simplicity, electrical and mechanical angles are the same. In this configuration the nine magnetic axes are equally arranged along all 360 degrees and they can not be overlapped by mirroring. The fundamental time variant MMF waveform of each phase are:

$$U_1 = \hat{U} \ \sin(\omega t) \cdot \sin(\alpha) \tag{2.22}$$

$$U_2 = \hat{U} \ \sin\left(\omega t - \frac{2\pi}{9}\right) \cdot \sin\left(\alpha - \frac{2\pi}{9}\right) \tag{2.23}$$

$$U_3 = \hat{U} \ \sin\left(\omega t - \frac{4\pi}{9}\right) \cdot \sin\left(\alpha - \frac{4\pi}{9}\right) \tag{2.24}$$

$$U_4 = \hat{U} \ \sin\left(\omega t - \frac{6\pi}{9}\right) \cdot \sin\left(\alpha - \frac{6\pi}{9}\right) \tag{2.25}$$

$$U_5 = \hat{U} \ \sin\left(\omega t - \frac{8\pi}{9}\right) \cdot \sin\left(\alpha - \frac{8\pi}{9}\right) \tag{2.26}$$

$$U_6 = \hat{U} \ \sin\left(\omega t - \frac{10\pi}{9}\right) \cdot \sin\left(\alpha - \frac{10\pi}{9}\right) \tag{2.27}$$

$$U_7 = \hat{U} \ \sin\left(\omega t - \frac{12\pi}{9}\right) \cdot \sin\left(\alpha - \frac{12\pi}{9}\right) \tag{2.28}$$

$$U_8 = \hat{U} \ \sin\left(\omega t - \frac{14\pi}{9}\right) \cdot \sin\left(\alpha - \frac{14\pi}{9}\right) \tag{2.29}$$

$$U_9 = \hat{U} \ \sin\left(\omega t - \frac{16\pi}{9}\right) \cdot \sin\left(\alpha - \frac{16\pi}{9}\right) \tag{2.30}$$

by applying 2.18 and remembering that $\sin(\alpha)\cdot\sin(\beta)=\frac{1}{2}[\cos(\alpha-\beta)-\cos(\alpha+\beta)]$, it is possible to obtain the resulting MMF fundamental:

$$\begin{aligned}
U_{tot} =& \frac{1}{2}\hat{U}\left(\cos(\omega t-\alpha)-\cancel{\cos\left(\omega t+\alpha-\frac{8\pi}{9}\right)}\right)+\\
&\frac{1}{2}\hat{U}\left(\cos(\omega t-\alpha)-\cancel{\cos\left(\omega t+\alpha-\frac{20\pi}{9}\right)}\right)+\\
&\frac{1}{2}\hat{U}\left(\cos(\omega t-\alpha)-\cancel{\cos\left(\omega t+\alpha-\frac{32\pi}{9}\right)}\right)+\\
&\frac{1}{2}\hat{U}\left(\cos(\omega t-\alpha)-\cancel{\cos(\omega t+\alpha)}\right)+\\
&\frac{1}{2}\hat{U}\left(\cos(\omega t-\alpha)-\cancel{\cos\left(\omega t+\alpha-\frac{12\pi}{9}\right)}\right)+\\
&\frac{1}{2}\hat{U}\left(\cos(\omega t-\alpha)-\cancel{\cos\left(\omega t+\alpha-\frac{24\pi}{9}\right)}\right)+\\
&\frac{1}{2}\hat{U}\left(\cos(\omega t-\alpha)-\cancel{\cos\left(\omega t+\alpha-\frac{4\pi}{9}\right)}\right)+\\
&\frac{1}{2}\hat{U}\left(\cos(\omega t-\alpha)-\cancel{\cos\left(\omega t+\alpha-\frac{16\pi}{9}\right)}\right)+\\
&\frac{1}{2}\hat{U}\left(\cos(\omega t-\alpha)-\cancel{\cos\left(\omega t+\alpha-\frac{28\pi}{9}\right)}\right)\\
=&\frac{9}{2}\hat{U}\cos(\omega t-\alpha)
\end{aligned}\tag{2.31}$$

The sum of all barred elements in 2.31 is equal to zero because in threes is the sum of three vectors shifted by 120 degree each other. It can be noticed that the maximum value of the fundamental MMF waveform is higher than the three-phase case. This suggests that, by using this configuration, the machine will be magnetically divided in nine parts with one-ninth of magnetic load each. This calculation could be done for every higher harmonics order but is not addressed here since, as already mentioned, the harmonic content is very low indeed according to [15] the present harmonics are :

$$\nu = 2\ km \pm 1 \qquad\qquad k\in\mathbb{Z} \tag{2.32}$$

2.3.2 3x3-phase system

In this configuration, it is interesting to consider three set of 3-phase with 3 star point consistent with the case shown in 2.5a, with a reduced system as as indicated in [18]. Therefore from 2.17 the angular displacement between the three sets of 3-phase, with $p=1$ and $m=9$ result:

$$\begin{aligned}
\alpha_{ph\ red} &= \frac{\pi}{m\cdot p}\\
&= \frac{\pi}{9} = 20°
\end{aligned}\tag{2.33}$$

The difference between the case reported in 2.3.1 is that the MMF related to the phase number 3, 6, 9 are electrically shifted by 180 degree.

$$U_1 = \hat{U}\ \sin(\omega t) \cdot \sin(\alpha) \tag{2.34}$$

$$U_2 = \hat{U}\ \sin\left(\omega t - \frac{2\pi}{9}\right) \cdot \sin\left(\alpha - \frac{2\pi}{9}\right) \tag{2.35}$$

$$U_3 = \hat{U}\ \sin\left(\omega t - \frac{4\pi}{9}\right) \cdot \sin\left(\alpha - \frac{4\pi}{9} + \pi\right) \tag{2.36}$$

$$U_4 = \hat{U}\ \sin\left(\omega t - \frac{6\pi}{9}\right) \cdot \sin\left(\alpha - \frac{6\pi}{9}\right) \tag{2.37}$$

$$U_5 = \hat{U}\ \sin\left(\omega t - \frac{8\pi}{9}\right) \cdot \sin\left(\alpha - \frac{8\pi}{9}\right) \tag{2.38}$$

$$U_6 = \hat{U}\ \sin\left(\omega t - \frac{10\pi}{9}\right) \cdot \sin\left(\alpha - \frac{10\pi}{9} + \pi\right) \tag{2.39}$$

$$U_7 = \hat{U}\ \sin\left(\omega t - \frac{12\pi}{9}\right) \cdot \sin\left(\alpha - \frac{12\pi}{9}\right) \tag{2.40}$$

$$U_8 = \hat{U}\ \sin\left(\omega t - \frac{14\pi}{9}\right) \cdot \sin\left(\alpha - \frac{14\pi}{9}\right) \tag{2.41}$$

$$U_9 = \hat{U}\ \sin\left(\omega t - \frac{16\pi}{9}\right) \cdot \sin\left(\alpha - \frac{16\pi}{9} + \pi\right) \tag{2.42}$$

By applying 2.18 the calculations are similar to 2.31: after doing the simplifications arising from the new angular displacement the last step is reported in 2.43:

$$\begin{aligned} U_{tot} =& -\frac{1}{2}\hat{U}\left(\cos(\omega t - \alpha)\right) + \frac{1}{2}\hat{U}\left(\cos(\omega t - \alpha)\right) + \frac{1}{2}\hat{U}\left(\cos(\omega t - \alpha - \pi)\right) + \dots \\ \dots& -\frac{1}{2}\hat{U}\left(\cos(\omega t - \alpha)\right) + \frac{1}{2}\hat{U}\left(\cos(\omega t - \alpha)\right) + \frac{1}{2}\hat{U}\left(\cos(\omega t - \alpha - \pi)\right) + \dots \\ \dots& -\frac{1}{2}\hat{U}\left(\cos(\omega t - \alpha)\right) + \frac{1}{2}\hat{U}\left(\cos(\omega t - \alpha)\right) + \frac{1}{2}\hat{U}\left(\cos(\omega t - \alpha - \pi)\right) = \\ =& -\frac{3}{2}\hat{U}\cos(\omega t - \alpha) \end{aligned} \tag{2.43}$$

It can be notice that 2.43 is the same case described in 2.3.1 with $m = 3$ instead $m = 9$. This solution maintains the advantage of the multi-phase systems described in 1 but is similar to the classical three-phase case from the magnetic point of view. Indeed the harmonics present do not follow the equation 2.32 but they are the same as three-phase case [4] i.e. :

- All systems of multiples of three are eliminated
- Harmonics order 7,13,19 only synchronous
- Harmonic order 5,11,17 form only inverse fields

These are the cases of the topologies shown in 2.5, but generally it is also possible to consider additional configurations with respect to those shown before, for example a reduced system in the 1x9-phase case and only a single star point in the 3x3-phase case. By adopting the same procedure as 2.3.1 and 2.3.2 the MMF formulation and the harmonic content are possible to calculate obtaining different characteristics. Finally the choice of the systems connection of the phases is related to the structure of the converter; for example if using standard converters is mandatory it must adopt a 3x3-phase system with three star point. Furthermore even the control strategy in fault condition should be considered for example after switching off the faulty subsystem, the 2x3-phases operation could be continued or if it will adopt a 1x9-phase system in the case of one phase is lost a specific control law must be implemented in order to maintain the same performance by using the the remaining 1x8-phase. These aspect are addressed in [12]. Always in [18] is reported that the probability for a total failure per hour of the electrical drive train is significantly less in 2.5b with respect in 2.5a; by considering also a more interesting magnetic configuration and a low harmonic content 2.31, 2.32, the configuration 2.5b is chosen for the next design of the machine.

2.4 Synthesis of distributed winding

The tool used to design and analyze the winding is the Star of Slot [8], [1]. It is the vectorial representation of the the electro-motive force (emf) induced in a conductor laying in a particular slot by a traveling flux-density waveform in the airgap. The electro-motive forces induced in different slots are equal in amplitude but have different phase angle. The star of slots is therefore a representation of the phasors in all the machine slots and so it is formed by Q phasors. They are numbered according to the number of the corresponding slot. In accordance with what obtained in 2.3, a symmetrical and balanced winding is required and these conditions are satisfy if:

- the amplitude of the main harmonic of the electro-motive force is the same for each phase
- the displacement between two adjacent phases is equal to $\frac{2\pi}{m}$ electrical radians

An important parameter, in this sense, is the machine periodicity that is the greatest common divisor (GCD) between Q and p :

$$t = GDC\{Q,p\} \tag{2.44}$$

The star of slot is an electrical representation of the machine therefore it characterised by Q/t spokes, with each spoke containing t phasors.If α_s is the mechanical slot angle than, the electrical angle between the phasors of two adjacent slots is $\alpha_s^e = p \cdot \alpha_s$ and consequently The angle between two spokes is:

$$\alpha_{ph} = \frac{2\pi}{Q/t} = \frac{\alpha_s^e}{p}\ t \tag{2.45}$$

When Q is a multiple of p, $t = p$ otherwise it is $t < p$. Normally only one phasor per spoke is drown, i.e. only a machine periodicity is represented in the star of slots.
In order to have a balanced and symmetrical winding the most important condition that have to be respected is:

$$\frac{Q}{m\ t} \text{ integer number} \tag{2.46}$$

This ensures that in the star of slots for each phase, an equal number of phasors can be assigned. The next step is to assign each phasor in the star of slots to a specific phase.The phasors that belong to the first phase are determined by drawing two opposite sectors, each of them covering an angle equal to:

$$\frac{\pi}{m} \tag{2.47}$$

The coil sides within one sector are connected with positive polarity, while the coil sides within the other sector are connected with negative polarity. For the other phases, it is enough to rotate the rest of the sectors by an angle of:

$$\frac{2\pi\ k}{m} \tag{2.48}$$

where k = 1,2,3,..,$(m-1)$ and to repeat the selection. Once the phase of each phasor is determined, it is fixed for the following steps of the design. In the figure 2.6 is reported a generic example to show what has just been said.

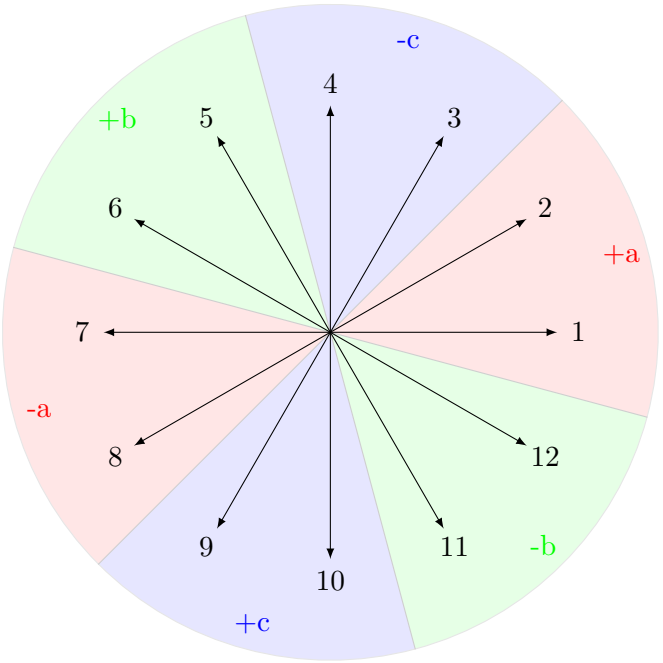

Figure 2.6 – Example of star of slot with $Q = 24$ slots, $2p = 4$ poles and $m = 3$ phases

It is worthwhile to note that if the number of phases m is an even number than each phase has again 2 sectors, positive negative, which are laid out 180 degree, but each phase is displaced by $180/m$ degrees from the next in the phase sequence. Then, in order to have a symmetrical and balanced winding, in this case the number of spokes for each phase in the star of slots must be even as well. So a more stringent condition is present:

$$\frac{Q}{m\ t} \text{ even} \tag{2.49}$$

2.4.1 Winding layout choice

The design of the winding consists in determine the combination of number of slots Q, number of slots per pole and per phase q and the number of pole pairs p. Generally this combination is not defined a priori and therefor an analysis among all possible combination is required to determine the best solution. Here are reported the criteria derived by the previous sections

- One of the most stronger limitation is reported in 2.46, in fact if a symmetrical distributed winding is required the number of slots Q must be a multiple of the number of phases m.

$$Q = m, 2m, 3m, ..., k\ m \qquad\qquad k \in \mathbb{Z} \tag{2.50}$$

- In order to obtain a near sinusoidal distribution of MMF at the airgap more than one slots per pole and per phase is required 2.2

$$q > 1 \tag{2.51}$$

  This causes a limitation in the possibilities because it becomes more and more difficult to satisfy this condition if the number of phases increases as already indicated in 2.2

- Fractional slot winding is used in order to improve the induced emf, indeed in this case the machine behaves as if it had more slots than it actually has [8], this solution is adopted for example in slow machines with lots of poles. As shown in 2.2, due to reasons related to sub-harmonics, fractional slot windings are acceptable in the field of induction machines only if q is in this form:

$$q = \text{integer} + 0.5 \tag{2.52}$$

By using an open source software developed by the Department of Industrial Engineering of the University of Padua called Dolomites (available in `https://sourceforge.net/p/dolomites/wiki/Home/`); it is possible to automatize both the synthesis and the analysis of a winding. Dolomites is based on the theory and formulations shown in 2.4 and a detailed description of the equations implemented in the software can be found in [1] by the developer. All the combination obtained are reported below: $Q = 54$ is taken as maximum available value because higher number of slot it would be difficult to realize in this particular case. By applying the conditions listed above, it is possible to exclude the not interest combinations.Generally the performance of a induction machine tends to decrease as the number of poles increases, therefore even the number of poles must be limited. The feasible solutions are marked in 2.8 with a green arrow. In 2.7 and 2.8 is reported also the winding factor k_w which is automatically calculated by Dolomites in a reference case as indicated in [1], but in the case under analysis it will precisely calculated in the next chapters. At this point the difficulty linked to 2.51 must be considered, because there is a risk of issues related to the building of the teeth and saturation of them during the work. As increasing of Q the teeth will be less large and nevertheless they will carry slightly less flux, this could be a problem. A very general preliminary criteria in order to avoid these problems during the design stage is indicated in [8] and [11]. Defining the slot pitch P_s as :

$$P_s = \frac{\pi\ D}{Q} \tag{2.53}$$

Qs	2p	kw	t	yq	q
9	2	0.945214	1	4	0,5
9	4	0.945214	1	2	0,25
9	6	0.866025	3	1	0,16666667
9	8	0.945214	1	1	0,125
9	10	0.945214	1	1	0,1
18	2	0.959795	1	9	1
18	4	0.945214	2	4	0,5
18	6	1	3	3	0,33333333
18	8	0.945214	2	2	0,25
18	10	0.735246	1	1	0,2
27	2	0.953852	1	13	1,5
27	4	0.940953	1	6	0,75
27	6	0.945214	3	4	0,5
27	8	0.940953	1	3	0,375
27	10	0.877327	1	2	0,3
36	2	0.956143	1	18	2
36	4	0.959795	2	9	1
36	6	0.965926	3	6	0,66666667
36	8	0.945214	4	4	0,5
36	10	0.923563	1	3	0,4
45	2	0.954542	1	22	2,5
45	4	0.954542	1	11	1,25
45	6	0.951436	3	7	0,83333333
45	8	0.940613	1	5	0,625
45	10	0.945214	5	4	0,5
54	2	0.955469	1	27	3
54	4	0.953852	2	13	1,5
54	6	0.959795	3	9	1
54	8	0.940953	2	6	0,75
54	10	0.949008	1	5	0,6

Figure 2.7 – All combination of Q, q, p for symmetrical winding with $m = 9$

	Qs	2p	kw	t	yq	q
	9	2	0.945214	1	4	0,5
	9	4	0.945214	1	2	0,25
	9	6	0.866025	3	1	0,16666667
	9	8	0.945214	1	1	0,125
	9	10	0.945214	1	1	0,1
➡	18	2	0.959795	1	9	1
	18	4	0.945214	2	4	0,5
	18	6	1	3	3	0,33333333
	18	8	0.945214	2	2	0,25
	18	10	0.735246	1	1	0,2
➡	27	2	0.953852	1	13	1,5
	27	4	0.940953	1	6	0,75
	27	6	0.945214	3	4	0,5
	27	8	0.940953	1	3	0,375
	27	10	0.877327	1	2	0,3
➡	36	2	0.956143	1	18	2
➡	36	4	0.959795	2	9	1
	36	6	0.965926	3	6	0,66666667
	36	8	0.945214	4	4	0,5
	36	10	0.923563	1	3	0,4
➡	45	2	0.954542	1	22	2,5
	45	4	0.954542	1	11	1,25
	45	6	0.951436	3	7	0,83333333
	45	8	0.940613	1	5	0,625
	45	10	0.945214	5	4	0,5
➡	54	2	0.955469	1	27	3
➡	54	4	0.953852	2	13	1,5
➡	54	6	0.959795	3	9	1
	54	8	0.940953	2	6	0,75
	54	10	0.949008	1	5	0,6

Figure 2.8 – Feasible combination of Q, q, p for symmetrical winding with $m = 9$

Qs	2p	kw	t	yq	q	ps
18	2	0.959795	1	9	1	0,0261
27	2	0.953852	1	13	1,5	0,0174
36	2	0.956143	1	18	2	0,013
36	4	0.959795	2	9	1	0,013
45	2	0.954542	1	22	2,5	0,0104
54	2	0.955469	1	27	3	0,0087
54	4	0.953852	2	13	1,5	0,0087
54	6	0.959795	3	9	1	0,0087

Figure 2.9 – Final choice of combination of Q, q, p for symmetrical winding with $m = 9$

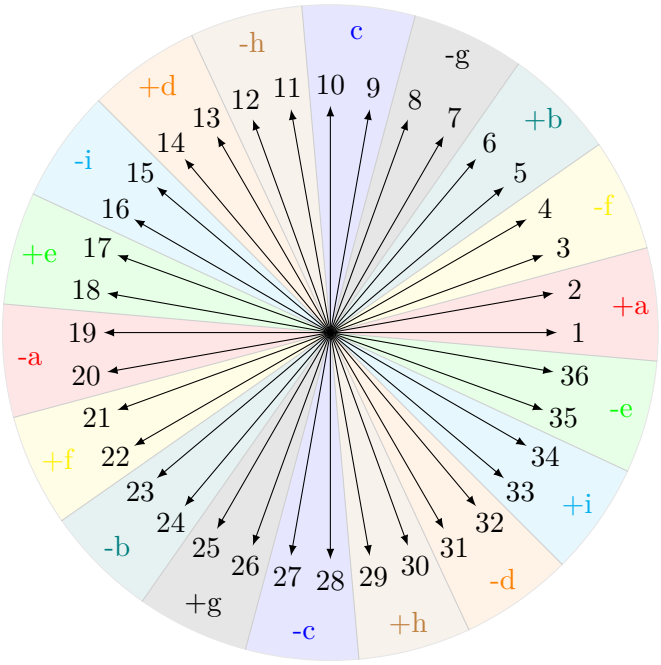

Figure 2.10 – Star of slot of the chosen winding Q=36,p=1, t = 1, m=9

where D is the inner diameter of the machine. The slot pitch value should stay in the range of values between 10 mm $< P_s <$ 40 mm, values referred from small machines (few KW) to very big machines (hundreds of KW). This condition, since is very general, should be it will also be checked later, but for the moment it is possible make the final choice of the winding based on it 2.9.
Therefore the final choice is 2.9:

- $Q = 36$
- $q = 2$
- $2p = 2$
- $P_s = 13$ mm

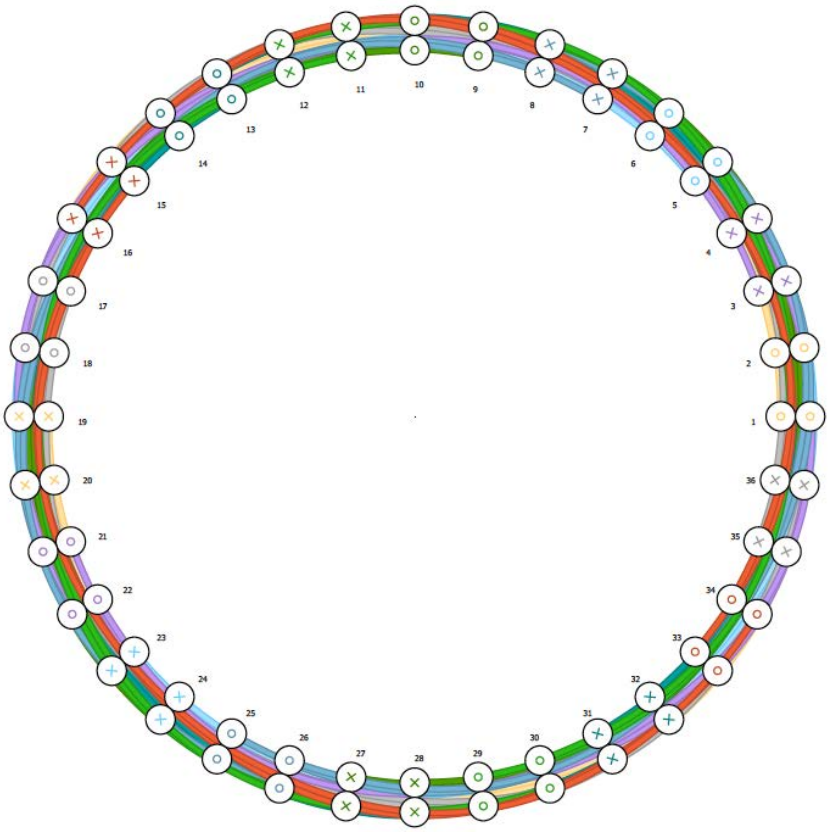

Figure 2.11 – Slot assignment Q, q, p for symmetrical winding with $m = 9$,full pitch, single layer

The winding coefficient is calculate as:

$$k_w = \frac{\sin q \ \frac{\alpha_s^e}{2}}{q \ \sin \frac{\alpha_s^e}{2}} = 0.996 \qquad \alpha_s^e = \frac{360°}{Q} = 10° \tag{2.54}$$

where α_s^e is the electrical angle between two adjacent stator slots.
Finally the symmetrical distributed winding for the nine-phase machine is defined: at this point it is possible to build the star of slot and assign to each slot the right phase 2.10. In 2.11 is reported the winding scheme, the picture shows a general case with the possibility of double layer winding but in this case a single layer winding is chosen and therefore a no-chorded winding with a coil throw $y_q = 18$ by using the equation 2.14. An analysis of electrical loading and of MMF waveform is reported in 2.13 calculated by Dolomites in the reference case mentioned mentioned in [1]. In this analysis a set of 9 symmetrical and balanced currents are imposed in the phases as shown in figure 2.12. In can be notice that the MMF waveform is made by 9 step, contributions of all phase according the values of the currents in each phase. As expected, the waveform is quasi-sinusoidal

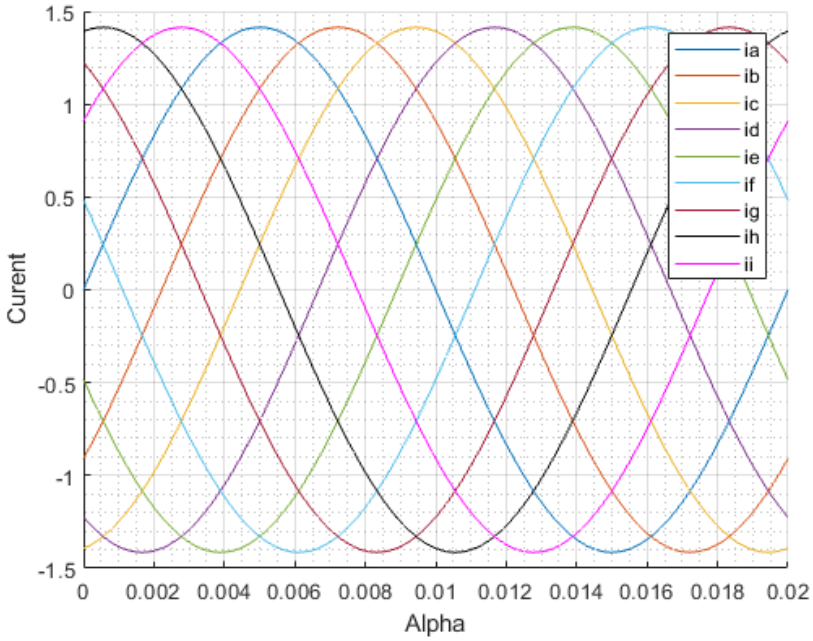

Figure 2.12 – Imposed currents for MMF analysis

.

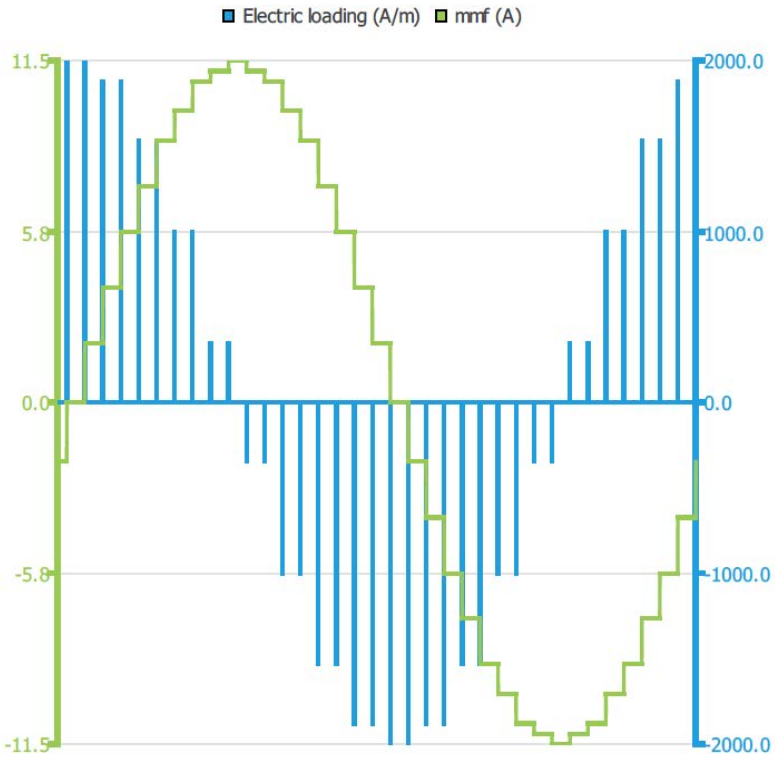

Figure 2.13 – Analysis of the chosen winding: Electrical load and MMF waveform using Dolomites

.

3 Design of the machine

The main geometry of the required nine-phase machine is calculated, starting from the classical theory of three-phase induction machines emphasizing when necessary the differences. The design procedure followed for this purpose is proposed in [8]. The design specifications are the same as the PM machine designed in [22] indeed the aim of this design is to propose a multi-phase induction machine as an alternative to those with technology based on permanent magnet. The design specification are reported in :

Table 3.1 – Design specifications of the 9-phase induction machine

Parameter	**Value**
Nominal power S	11 KWA
Nominal rotational speed n_0	3000 min^{-1}
Number of phases m	9
Phase voltage V_n	230 V

3.1 Main geometry of the machine

From the specifications reported in 3.1 a a preliminary sizing of the machine can be done. The set of Q, q,p was fixed in 2.4.1 and since the rotational speed is required by the design data, also the electrical frequency of work is fixed:

$$p = \frac{60\ f}{p} \qquad\qquad f = 50\,\text{Hz} \tag{3.1}$$

and also the the mechanical angular speed of the rotor:

$$\omega_m = \frac{2\pi\ n_0}{60} = 314.16\ \ \text{rad/s} \tag{3.2}$$

By supposing a reasonable value of the power factor $\cos(\phi) = 0.9$, an estimation of nominal output torque and maximum torque are calculated:

$$T_n = \frac{S\ \cos(\phi)}{\omega_m} = 32\,\text{N} \tag{3.3}$$

$$T_{max} \simeq 2.5\ T_n = 80\,\text{N} \tag{3.4}$$

The Possa's formulation gives the degree of utilization of the machine and so is taken as starting point of the machine's rotor but several different way could be used, for example the Essson's parameter [17].

$$\Phi = 1{,}3 \cdot 10^{-3}\ \frac{T_{max}^{0.55}}{p^{1.1}} = 0{,}0145\,\text{Wb} \tag{3.5}$$

The flux Φ can be also expressed as :

$$\Phi = B_g \cdot \frac{D\ L}{p} \tag{3.6}$$

where L is the length stack. By assuming from the past experience a reasonable values of $B_g = 0{,}8$ and $L/D = 0{,}8$ the main dimension and the pole pitch τ_p result:

- $D = 150\,\text{mm}$
- $L = 120\,\text{mm}$
- $\tau_p = \frac{\pi\ D}{2\pi} = 235{,}6\,\text{mm}$

In order to consider the presence of the insulation among the sheets a packing coefficient $k_{pack} = 0.96$ is considered, therefore the total iron length is $L_{fe} = L \cdot k_{pack}$

3.2 Stator geometry: Slots and back iron

Considering the fixed phase voltage V_n and the number of phases m the nominal phase current I_s results:

$$I_s = \frac{S}{m\ V_n} = 5{,}31\,\text{A} \tag{3.7}$$

I_s must be carried out by the conductors in the slot. A current density $J_s = 5\ \text{A/mm}^2$, typical value of the three-phase case, is assumed according to the design guideline [8], therefore the equivalent surface results:

$$S_{c\ eq} = \frac{I_s}{J_s} = 1{,}062\,\text{mm}^2 \tag{3.8}$$

The total number of conductor can be obtained by estimating the real voltage on the winding with $E = 0.97\ V_n$ and using:

$$N \simeq \frac{E\ \sqrt{2}}{\pi f\ \Phi\ k_w} \tag{3.9}$$

and the number of series conductor n_cs with:

$$n_{cs} = \frac{m\ N}{Q} \tag{3.10}$$

In the table 3.2 are reported all parameters of the winding. No parallel path are done because the current in the stator is low.

Table 3.2 – Characteristics of the final winding

q	Q	P_s	n_{cs}	N
2	36	13.1 mm	38	152

In order to realize the required conductor surface, two commercial elementary wires are taken with for having a easier wound process : diameter of the wires $d_c = 0.8$, and therefore the real equivalent conductor surface is:

$$S_c = \frac{2 \cdot \pi \cdot d_c^2}{4} = 1{,}005\,\text{mm}^2 \tag{3.11}$$

and the total surface copper in the slot results:

$$S_{cu\ slot} = n_{cs} \cdot S_c = 38{,}2\,\text{mm}^2 \tag{3.12}$$

Finally the by assuming a fill factor $k_{fill} = 0.42$ the total surface of the slot S_{slot} results :

$$S_{slot} = \frac{S_{cu\ slot}}{k_{fill}} = 90\,\text{mm}^2 \tag{3.13}$$

At this point the geometry of the slot must be drawn; in order to do this a possible criteria is to consider rectangular teeth so that they are able to carry evenly the flux. A trapezoidal stator slot results from this criteria.Other solution with their characteristic can be founded in [18]. The calculation of the quantities of the slot were calculated in MatLab by implementing the the geometrical formulation: the main dimensions of the slot are reported here:

- $w_{so} = 2$ mm : width of slot opening;
- $h_{so} = 2$ mm : high of slot opening;
- $r = 3.74$ mm : lower radius of the slot shape;
- $h_s = 15$ mm : total high of the slot;
- $w_t = 6.5$ mm : width of the tooth.

The formulation implemented in MatLab for calculate the high of the slot is :

$$h_s^2 + \frac{Q\ w_s\ h_s}{\pi} - \frac{Q\ S_{slot}}{\pi} = 0 \tag{3.14}$$

where $w_s = P_s - w_t$.
The last parameter that are involved in the stator dimension is the high of the back iron h_{bi}. The back iron is interested by only half of the total flux per pole Φ:

$$\Phi_{bi} = \frac{1}{2} \cdot \Phi \tag{3.15}$$

therefore by applying the Gauss's law and under the assumption of a value of flux density in back iron $B_{bi} = 1.5\,\text{T}$ from :

$$\Phi = h_{bi} \cdot B_{bi} \cdot L \tag{3.16}$$

it results $h_bi = 40\,\text{mm}$. Since at this point all dimension are calculate it is possible to obtain the value of the external diameter D_e:

$$D_e = D + 2h_s + 2h_{bi} = 260\,\text{mm} \tag{3.17}$$

3.3 Rotor geometry

Generally three types of rotors are possible in the field of the induction machine according to the performances and the power level required [8] [18]. The rotor type influences the electrical parameters of the machine and the performance as well. In this case a single cage rotor is chosen because of the low level of power and because there is not necessity of a great starting torque since the machines will be feed by converter. Here it is necessary to select a value

Table 3.3 – Possible type of rotors according the power level

P (KW)	Type
1 - 50	Single cage
50 - 500	Wound
50 - 5000	Double cage

of the airgap, this is a choice of the designer and it is possible to adopt a range indication founded in [18] i.e. $g = 0.5 - 2\,\text{mm}$ where the higher values are generally selected for big size machine. With this in mind the choice of the thickness airgap is $g = 0.8\,\text{mm}$. The number of rotor slots are freely selectable as long as it is avoided certain combination with the number of stator slot for avoid torque ripple and harmonics in MMF. The condition are:

- $Q_r \neq Q_s$;
- $|Q_r - Q_s| \neq 2p$;

As an alternative way, it is possible to select Q_r according to Q_s chosen before from tables derived from past experience in the design of this type of machines. An example of that could be found in in [8]. The value chosen for this design is $Q_r = 28$. The shape of the bars are important for the performance of the machine: for example a small bars has high resistance and therefore an high starting torque but a low efficiency. In this sense it must do a compromise between performance and minimisation of losses. Sever shape for rotor bars are discussed in [18] and [9]. Here for the machine under discussion a trapezoidal rotor slot is chosen. The current in the bar is obtained from:

$$I_{bar} \frac{m\ k_w\ N\ I_{sr}}{Q_r} = 230\,\text{A} \tag{3.18}$$

where I_{sr} is the rotor current reported to the stator and it is estimable with the active part of I_s i.e $I_{sr} = \cos(\phi) I_s = 4.72\,\text{A}$. The current density of the rotor bar is chosen very low i.e $J_r = 2\,\text{A}/\,\text{mm}^2$ this because the multi-phase machine permits lower amount of current in the bars and therefore with the same rotor surface it is possible to obtain a lower electrical resistance. The total rotor slot surface will be:

$$S_{bar} = \frac{I_{bar}}{J_r} = 110\,\text{mm}^2 \tag{3.19}$$

By using the same approach as 3.2 a MatLab script was written and the result are:

- $w_{sor} = 1\,\text{mm}$: width of rotor slot opening;
- $h_{sor} = 2\,\text{mm}$: high of rotor slot opening;
- $P_{sr} = 16.65\,\text{mm}$: rotor slot pitch;
- $r_r = 4\,\text{mm}$: radius of rotor bar shape;
- $h_r = 18\,\text{mm}$: high of rotor bar;
- $w_{er} = 6.13\,\text{mm}$: width of the slot's bottom edge.
- $w_{tr} = 7.33\,\text{mm}$: width of the rotor tooth.

A skewing of rotor bar is adopted in order to avoid synchronous torque phenomena caused by a non perfect magnetic linkage between rotor and stator. A skewing angle is freely selectable but some indications can be founded in [8]. In this case the skewing angle, α^e_{skew}, is chosen equal to one rotor slot angle, therefore:

$$\alpha^e_{skew} = \frac{2\pi}{Q} = 0.2244 \text{ radians} \tag{3.20}$$

and the skewing coefficient is:

$$k_{skew} = \frac{\sin \frac{\alpha^e_{skew}}{2}}{\frac{\alpha^e_{skew}}{2}} \tag{3.21}$$

The last step is sizing the two short circuit rings. The ring current is expressed as:

$$I_{ring} = \frac{I_{bar}\ Q_r}{2p\ \pi} = 1025\,\text{A} \tag{3.22}$$

Assumed a current density $J_{ring} = 3\,\text{A}/\,\text{mm}^2$ the ring surface is :

$$S_{ring} = \frac{I_{ring}}{J_{ring}} = 340\,\text{mm}^2 \tag{3.23}$$

and the dimensions were chosen $20\,\text{cm} \times 17\,\text{cm}$. Is called D_r the ring's diameter measured in the middle point.

$$D_r = D - 2g - h_r = 130.4\,\text{mm} \tag{3.24}$$

3.4 Machine Geometry

The geometry was drawn with the CAD tool of F.E.M.M., open source software used in the next chapter for address the FEA analysis of the Machine. In this passage it is important to reproduce the design geometry as accurate as possible in order to having the best results in the solution. The geometry and some detail are reported in 3.1 and 3.2.

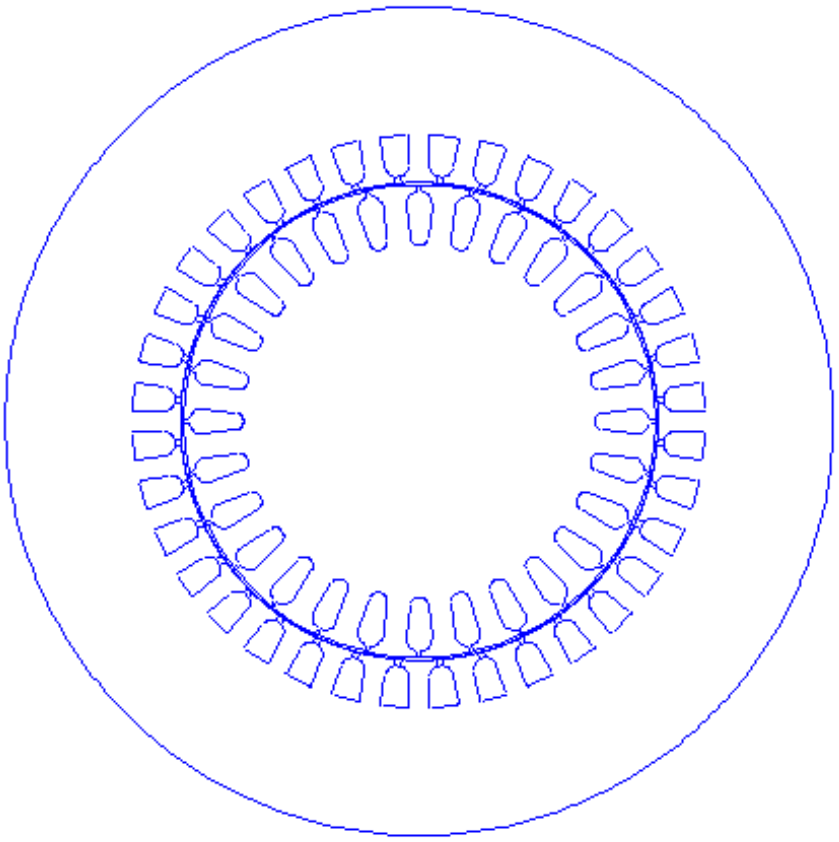

Figure 3.1 – Stator and rotor final geometry

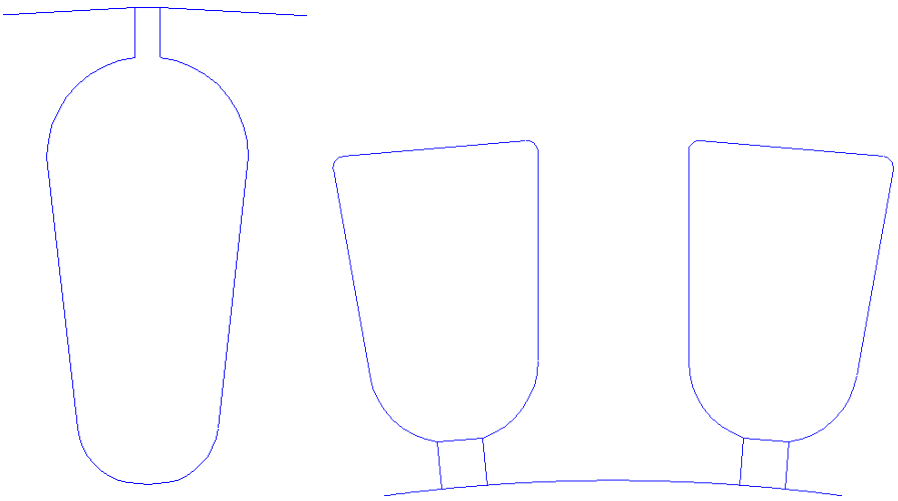

(a) *Detail of rotor bar* **(b)** *Detail of stator slot*

Figure 3.2 – Geometry details

4 Analytical analysis

The analytical analysis is an important step for having both a fist prediction of the machine's performance and for possible changes in order to improve it. Furthermore this step it will useful for comparing and confirm the FEA result of the 6. The analytical model is very simplified because no-precise calculation is required here.

4.1 Magnetic circuit

The magnetic circuit analysis is performed by dividing the machine into four main parts. Each part is considered in order to check the maximum flux density and calculate the magnetic voltage drop i.e. the required current (Amps-turns A) for magnetize each part.This study allows to estimate the value of the magnetization current and magnetize inductance which will be compared with those obtained by the FEMM test. For the calculation of the the magnetic field corresponding to the flux density it is used the data sheet downloadable from `http://www.voestalpine.com/division_stahl/content/download/34049/362555/file/DS`. The approach follows the procedure presented in [8]

Airgap
The current needed to magnetize the airgap is obtainable by knowing its thickness g, the flux density B_g and the Carter's coefficient k_c. The Carter's coefficient can be approximately calculated by:

$$\frac{P_s}{P_s + g - \frac{3}{4}\, w_{so}} = 1.0568 \tag{4.1}$$

so, it is possible to calculate:

$$A_g = \frac{B_g}{\mu_0} \cdot g' = 490\ A \tag{4.2}$$

where $g' = g \cdot k_c$.

Stator tooth
The flux density at stator tooth can be calculated as:

$$B_{tooth} = \frac{B_g \cdot P_s \cdot L_{stk}}{L_{fe}} = 1.5\,\mathrm{T} \tag{4.3}$$

From the B-H curve it can be obtained $H_{tooth} = 1180\,\mathrm{A/m}$ and therefore:

$$A_{tooth} = H_{tooth} \cdot h_s = 18\,\mathrm{A} \tag{4.4}$$

where h_s tooth high.

Rotor tooth
By adopting a calculation similar to the previous one the flux density is:

$$B_{tr} = \frac{B_g \cdot P_{sr} \cdot L_{stk}}{w_{tr} \cdot L_{fe}} = 1.81\ T \tag{4.5}$$

Where P_{sr} rotor pole pitch and w_{tr} is the rotor tooth thickness.From the B-H curve results $H_{tr} = 10000$ A/m results:

$$A_{tr} = H_{tr} \cdot h_{tr} = 180\ A \tag{4.6}$$

where h_t is the high of the rotor tooth.

Back iron
Since the analytical analysis is a preliminary investigation, it is possible to adopt a simplified approach for calculating the contribution of the stator back iron. The back iron is not uniformly interested by the same flux density, but moving from the interpolar axis towards the polar axis it reduces and a accurate calculation would be necessary for taking into account of this reduction. However the simplified approach can be used by decreasing the maximum flux density B_{bi} by $85 - 90$ % and by using this average value along all back iron length.

$$B^* = 0.85 \cdot B_{bi} = 0.9 \cdot 1.45 = 1.3\ T \tag{4.7}$$

than from B-H curve it results $H_{bi} = 200\,\mathrm{A/m}$ and finally:

$$A_{bi} = H_{bi} \cdot l_{bi} = 34.4\ A \tag{4.8}$$

where l_{bi} is the length of the back iron under a pole in its middle position.

$$l_{bi} = \frac{\pi \cdot (D_e - h_{bi})}{2 \cdot 2p} = 172\,\mathrm{mm} \tag{4.9}$$

Total
By summing all contribution of Amps-turns founded in the magnetic circuit it is possible to obtain the total current needed for magnetize the machine and therefore it is possible to calculate the magnetize current at no-load:

$$\sum H \cdot l = \frac{m \cdot k_w \cdot N \cdot \sqrt{2} \cdot \hat{I}_\mu}{\pi \cdot 2p} = 725\ A \tag{4.10}$$

and than $\hat{I}_\mu = 2.87\,\mathrm{A}$.
Finally it is possible to calculate the magnetizing inductance as:

$$L_m = \frac{\hat{\Lambda}}{\hat{I}_\mu} = \frac{m \cdot \mu_0 \cdot}{\pi} \cdot \left(\frac{k_w \cdot N}{2p}\right)^2 \cdot \frac{D \cdot L}{g''} = 0.330\ \mathrm{H} \tag{4.11}$$

where $g'' = g' \cdot k_{sat} = 1.47$. which is the ratio between the current needed to magnetize all machine and the airgap. In the computation it is neglected the contribution for the magnetization of the rotor joke. This is usually small because the surface that the flux meets here is very large with respect the stator back iron. However in a two-pole machine there would be the presence of the magnetization of the shaft; even if in [18] is reported that the shaft of the machine is far more reluctive than the rotor sheet, and furthermore, the shaft is often jagged at the rotor bundle, thus there are air spots between the rotor iron and the shaft,therefore no flux penetrate the rotor shaft, it would be interest to estimate this contribution.

4.1.1 Leakage inductances

The main leakage inductances are calculate in this section. The calculation will be based on semi-empirical formulations on a simplified geometry of machine's shapes which give an estimation of the principal contribution. The following equation can be founded in [8].

Leakage inductances of stator slots
The stator slot in 3.2 is simplified by considering it as trapezoidal and the stator slot leakage inductance results:

$$L_{\sigma slot} = \mu_0 \cdot L \cdot n_{cs}^2 \cdot q \cdot 2p \cdot k_{slot} = 2.01\text{mH} \tag{4.12}$$

where k_{slot} is a geometrical parameter which for this particular shape is equal to 0.41.

Leakage inductances of rotor slots
The machine is designed with a squirrel rotor cage in particular with a single trapezoidal bar. As in the previous case the slot coefficient is calculated; on this particular shape results $k_{slot\ r} = 2.64$. The rotor slot leakage inductance is:

$$L_{\sigma\ r} = \frac{m}{Q_r} \cdot \left(\frac{k_w\ N}{k_{skew}}\right)^2 \cdot \mu_0 \cdot L \cdot k_{slot\ r} = 3\text{mH} \tag{4.13}$$

Zig-zag leakage inductance
The zig-zag leakage inductance is due to the interaction between stator and rotor teeth:

$$L_{\sigma zz} = \mu_0 \cdot L_{stk} \cdot 2p \cdot q \cdot n_{cs}^2 \cdot k_w^2 \cdot \left[\frac{(w_{t1} + w_{t2})^2}{3\ g \cdot 4(P_s + P_{sr})}\right] = 0.72\ \text{mH} \tag{4.14}$$

Where P_s e P_{sr} are the stator and rotor slot pitch obtained in chapter 3 and $w_{t1} = P_s - w_{so} =$ 11.1 mm e $w_{t2} = P_{sr} - w_{sor} = 16.65$ mm the distances between the stator and rotor slots.

Skewing leakage inductance
This leakage is due to the skewing of the rotor bars in order to avoid synchronous torque phenomena and involves a non perfect magnetic linkage between rotor and stator [20]. The skewing angle is calculated in and it is $\alpha_{skew}^e = 0.2244$ radians, and the skewing factor is $k_{skew} = 0.997$. Therefore the skewing leakage inductance results :

$$k_{skw} = \frac{\sin(\frac{\alpha_{skw}^e}{2})}{\frac{\alpha_{skw}^e}{2}} = 0.9987 \tag{4.15}$$

$$L_{\sigma skw} = L_m \cdot (1 - k_{skw}^2) = 1.79\text{mH} \tag{4.16}$$

End-winding leakage inductance
By simplifying once again the calculation, it is possible to adopt a semi-empirical equation [20]:

$$L_{\sigma ew} = \mu_0 \cdot L_{ew} \cdot 2p \cdot q^2 \cdot n_{cs}^2 \cdot \lambda_{ew} = 1.9\text{mH} \tag{4.17}$$

where for the distributed imbricated winding α_{ew} =0.35 and $L_{ew} = 2.5\ D/p$= 0.375 m is the estimation of the total length of the end-winding.

Belt leakage inductance
This leakage flux results from the non-sinusoidal MMF distribution of the winding. To compute it, some data are necessary:

$$\frac{Q + Q_r}{2} = 32 \tag{4.18}$$

and by using it as input from the diagram 4.1 results $k_B = 1$. The belt leakage inductance is:

$$L_{\sigma\ belt} = 3{,}65 \cdot 10^{-3} \cdot L_m \cdot k_B = 1.1\text{mH} \tag{4.19}$$

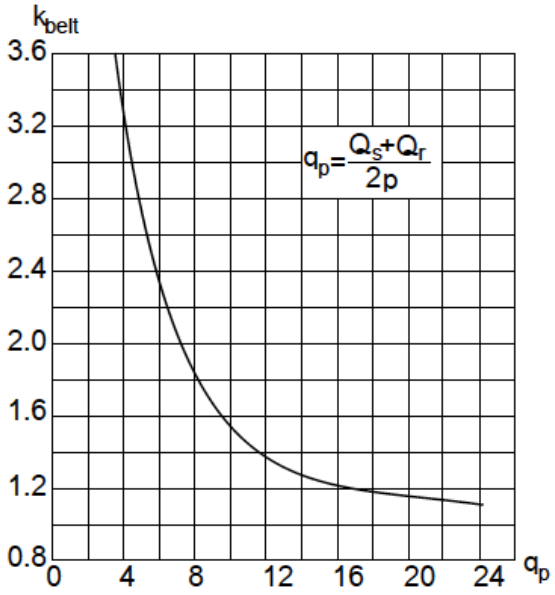

Figure 4.1 – Belt constant

Total
Finally the total leakage inductance is :

$$L_\sigma = L_{\sigma slot} + L_{\sigma r} + L_{\sigma zz} + L_{\sigma skw} + L_{\sigma ew} + L_{\sigma belt} = 9.51\text{mH} \tag{4.20}$$

This final result referred to main inductance L_m is :

$$\frac{L_\sigma}{L_m} \simeq 3\% \tag{4.21}$$

Usually for a three-phase IM this ratio is about 10%; in the case under analysis is lower but acceptable, since the total leakage inductance is quite low it is expected an high value of the maximum torque.

4.1.2 Losses

In this section are reported the main step for estimate the losses of the machine.

Stator copper losses
The stator winding material is copper and the reference working temperature is assumed at 120 °C. The characteristics of winding are reported here:

- $L = 0.120$ m : stack length;
- $L_{ew} = 0.375$ m : end-winding length;
- $L_c = L + L_{ew} = 0.495$ m : total copper conductor length;
- $N = 152$: total number of conductor;
- $n_c = 38$: number of series conductor;
- $S_c = 1.004$ mm : copper surface.

The stator copper resistance R_s is calculated as:

$$R_s = \rho_{cu} \frac{N\ L_c}{S_c} = 1.87\Omega \tag{4.22}$$

with $\rho_{cu} = 0{,}025 \cdot 10^{-6}\Omega\cdot$ at 120 °C. The stator joule losses are:

$$P_{js} = m \cdot R_s \cdot I_s^2 = 473\,\mathrm{W} \tag{4.23}$$

Stator copper losses
The main contribution to the iron losses comes from the teeth and the stator back iron. As calculated in the first part of the analytical analysis in this chapter these two part of the machine are interested a certain flux density B which corresponds to a certain specific loss obtainable from the specific losses characteristics find on the data sheet of the lamination at 50 Hz:

- $B_{tooth} = 1.5\,\mathrm{T} \longrightarrow 2\,\mathrm{W/kg}$
- $B_{bi} = 1.42\ T \longrightarrow 1.5\,\mathrm{W/kg}$

Once these value are obtained, the calculation of the total weight of the teeth and of the stator back iron are performed:

$$G_{teeth} = \gamma_{iron} \cdot Q \cdot w_t \cdot h_s \cdot L_{iron} = 3.23\,\mathrm{kg} \tag{4.24}$$

$$G_{bi} = \gamma_{iron} \frac{\pi}{4} \cdot \left[D_e^2 - \left(D_e - 2h_{bi}\right)^2\right] \cdot L_{iron} = 25\,\mathrm{kg} \tag{4.25}$$

where γ_{iron} =7800 kg/m^3.The total power dissipated in the iron is:

$$P_{iron} = (2) \cdot 2 \cdot 3.23 + (1.5) \cdot 1.5 \cdot 25 = 70\,\mathrm{W} \tag{4.26}$$

The coefficient (2) and (1.5) are inserted for taking into account of the no-perfect insulation in the lamination due to the manufacture [8].

Rotor copper losses
The rotor bars are made by aluminium die-cast and the reference temperature is the same

of the stator. The rotor bar current is calculated in 3.18 and therefore the ring current is expressed as:

$$I_{ring} = \frac{I_{bar}\ Q_r}{2p\ \pi} = 1025\,\mathrm{A} \tag{4.27}$$

Assumed a current density $J_{ring} = 3\,\mathrm{A/mm^2}$ the ring surface is :

$$S_{ring} = \frac{I_{ring}}{J_{ring}} = 340\,\mathrm{mm^2} \tag{4.28}$$

and the dimensions were chosen $20\,\mathrm{cm} \times 17\,\mathrm{cm}$. The rotor losses can be computed:

$$P_{jr} = Q_r \cdot \rho_{Al} \frac{L}{S_{bar}} \cdot I_{bar}^2 + 2\rho_{al} \cdot \frac{\pi\,(D_r - h_r)}{S_{ring}} \cdot I_{ring}^2 = 65 + 101\,\mathrm{W} \tag{4.29}$$

the total rotor resistance is obtained with:

$$R_r = \frac{P_{jr}}{m \cdot I_{sr}^2} = 0.82\Omega \tag{4.30}$$

In 5.29 $\rho_{al} = 0{,}04 \cdot 10^{-6}\Omega\cdot$ at $120\,^{\circ}\mathrm{C}$; two contributions of bar losses and ring losses are visible.

Mechanical losses
By using a semi-empirical equation the mechanical losses can be estimated as:

$$P_{mecc} = (0.6 - 0.8) \cdot P_{in\ (kW)} \cdot \sqrt{n_{(rpm)}} = 325\,\mathrm{W} \tag{4.31}$$

By using $P_{in} = 9.9\,\mathrm{W}$

Total
The total losses are:

$$P_{tot} = P_{js} + P_{iron} + P_{jr} + P_{mecc} = 1030\,\mathrm{W} \tag{4.32}$$

A supplementary 10% is added in order to taking into account the contribution of the additional losses i.e $P_{add} = 103\,\mathrm{W}$. Therefore the total losses of the machine result finally:

$$P_{loss} = P_{tot} + P_{add} = 1140\,\mathrm{W} \tag{4.33}$$

At this point it is possible to calculate the efficiency of the machine at the rated working point with:

$$\eta = \frac{P_{out}}{P_{in}} = \frac{S \cdot \cos\phi - P_{loss}}{S \cdot \cos\phi} = 88\% \tag{4.34}$$

An estimation of the nominal slip is possible from the estimation of the losses according to:

$$s = \frac{P_{jr}}{P_{out} + P_{mecc} + P_{P_{jr}}} = 1.6\% \tag{4.35}$$

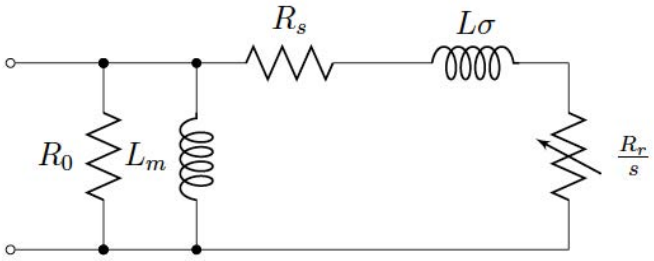

Figure 4.2 – Equivalent simplified circuit of IM machine

4.2 Mechanical characteristic

From the machine's parameters obtained in the analytical analysis it is possible to build the equivalent single-phase simplified circuit in 4.2. By applying the definition of the electromagnetic torque of the machine it can be write the torque with the dependence of the slip:

$$T_{em} = \frac{m \cdot R_r \frac{1-s}{s} \cdot I_{sr}^2}{\omega_m} \tag{4.36}$$

With the implementation of a MatLab code it is possible to calculate the mechanical characteristic of the machine obtained from analytical approach 4.3; this will be compared with the FEA results.

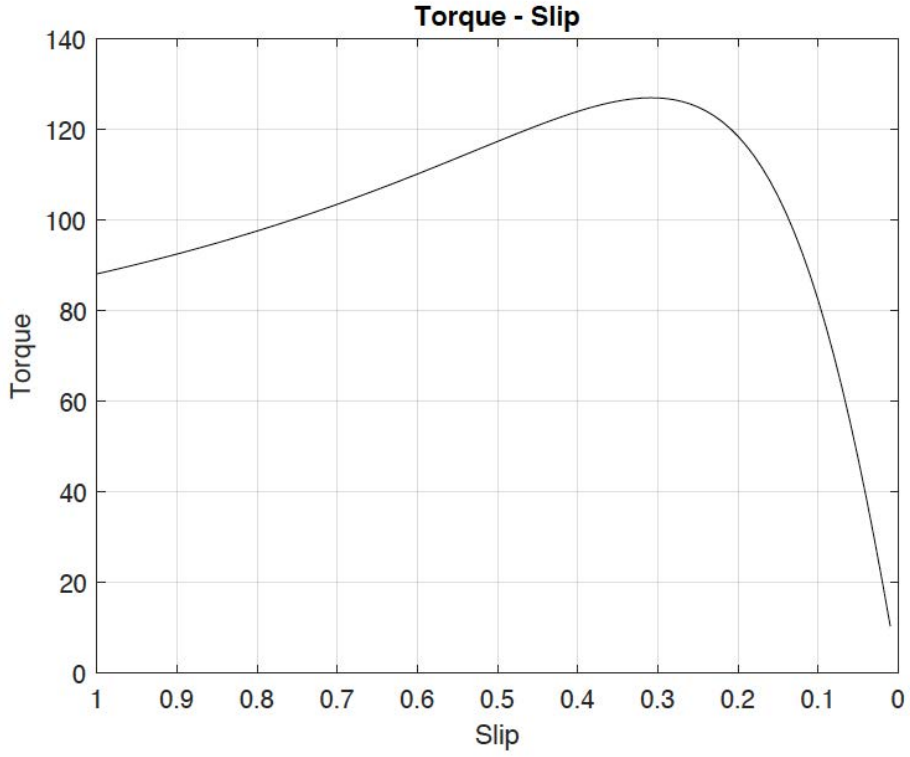

Figure 4.3 – Analytical mechanical characteristic

5 Finite element analysis

The Finite element analysis shown in this chapter is performed with open source software F.E.M.M. [16] The finite element analysis requires a high computation time. A good compromise is to combine analytical and FE models so as to get advantages and to reduce the drawbacks, in this way the simulation time is reduced, and the iron saturation phenomena are better considered. The flux lines are for the most part 2-D lines, therefore a 2-D analysis is generally satisfactory. Then, a 3-D correction is needed so as to include end-winding and ring resistances and inductances, skewing effect, and so on. The motor parameters are calculated by simulating the no-load test and the locked rotor test by impressing appropriate currents, than the equivalent circuit of the machine is build and analyzed with impressed voltage for all following computations. The analysis performed follows the approach shown in [3] and [6] for the three-phase case; in this chapter it will be extend to the nine-phase case. The management of the execution of both tests is performed through MatLab scripts, both for the assignment of currents in the slots and for the collection of data for the post-processing.

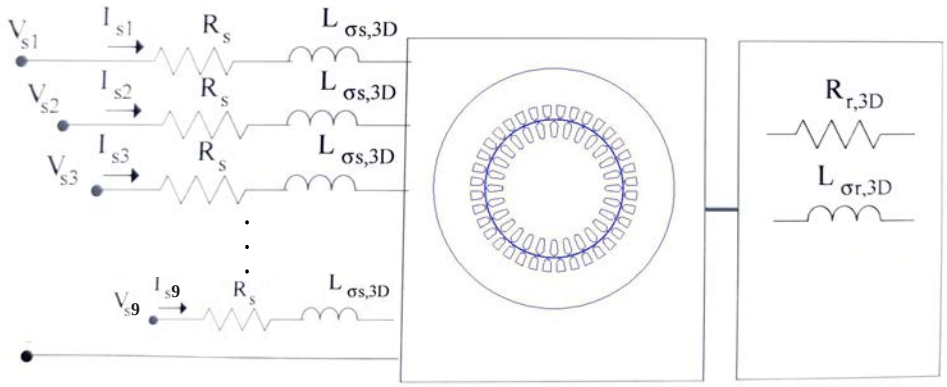

Figure 5.1 – FEM analysis scheme of nine-phase machine

5.1 No-load simulation

The machine is analyzed in the rotor reference frame. In fact considering the rotor running without load, the slip is equal to zero and therefore the frequency results to be equal to zero as well. Thus, FE magnetostatic simulations are carried out, where the field source is the current imposed in the stator slots. There is no current induced in the rotor bars, the rotor is seen only as a non-linear magnetic circuit where the magnetic flux lines close. A set of nine

currents fixed in time t when the phase a has the maximum values so that its magnetic axis is located along the horizontal axes.

$$i_a = \sqrt{2}\ I_s \cos(0) \tag{5.1}$$

$$i_b = \sqrt{2}\ I_s \cos\left(-\frac{2\pi}{9}\right) \tag{5.2}$$

$$i_c = \sqrt{2}\ I_s \cos\left(-\frac{4\pi}{9}\right) \tag{5.3}$$

$$i_d = \sqrt{2}\ I_s \cos\left(-\frac{6\pi}{9}\right) \tag{5.4}$$

$$i_e = \sqrt{2}\ I_s \cos\left(-\frac{8\pi}{9}\right) \tag{5.5}$$

$$i_f = \sqrt{2}\ I_s \cos\left(-\frac{10\pi}{9}\right) \tag{5.6}$$

$$i_g = \sqrt{2}\ I_s \cos\left(-\frac{12\pi}{9}\right) \tag{5.7}$$

$$i_h = \sqrt{2}\ I_s \cos\left(-\frac{14\pi}{9}\right) \tag{5.8}$$

$$i_i = \sqrt{2}\ I_s \cos\left(-\frac{16\pi}{9}\right) \tag{5.9}$$

The field lines obtained can be viewed in the figures 5.2, note that the magnetic axis of the phase a is correctly positioned on the horizontal axis, this is because in a hypothetical field oriented control (FOC) only the d-axes current produces the magnetic flux.The problem solved is non-linear and characterized by time-invariant quantities. One of the parameters obtained in no-load test is The stator fluxes linkage are calculated in F.E.M.M in according to 5.10 and than the the magnetizing inductance L_m of the machine is obtained [7].

$$\Lambda_{oj} = 2\ p\ L\ n_{cs} \sum_{q=1}^{Q/2p}\ k_{jq} \frac{1}{S_{slot}} \int_{S_{slot}} A_z\ dS \qquad\qquad j = a,b,c,...,i \tag{5.10}$$

Where k_{jq} is the corresponded line of the slot matrix for each phase [8]. In order to do this, three possibilities are reported here:

- With the flux linkage with a-phase λ_a:

$$L_m = \frac{\lambda_a}{\hat{I}} \tag{5.11}$$

  This formulation is valid only in the linear conditions.

- With Calculation by magnetic energy W:

$$L_m = \frac{2}{9} \cdot \left(\frac{2\ W}{\hat{I}^2}\right) \tag{5.12}$$

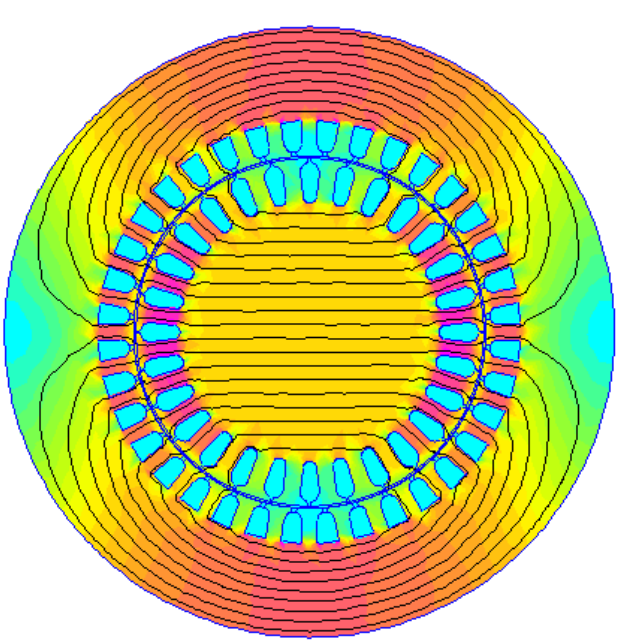

(a) *Flux density map*

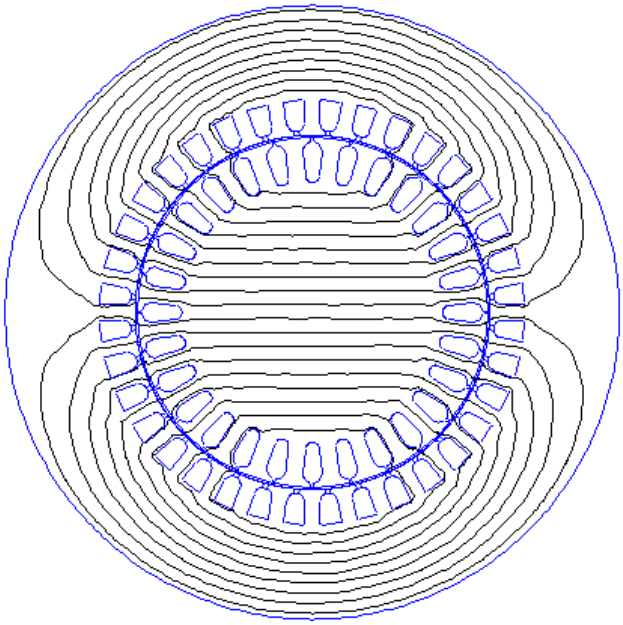

(b) *Flux line: no load test*

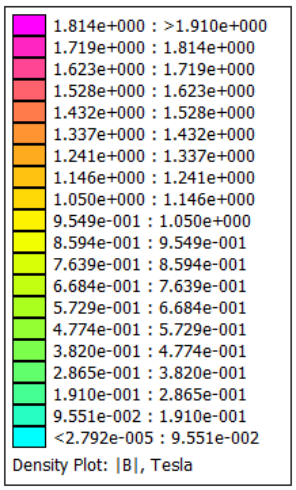

(c) *Legend*

Figure 5.2 – No load test simulation

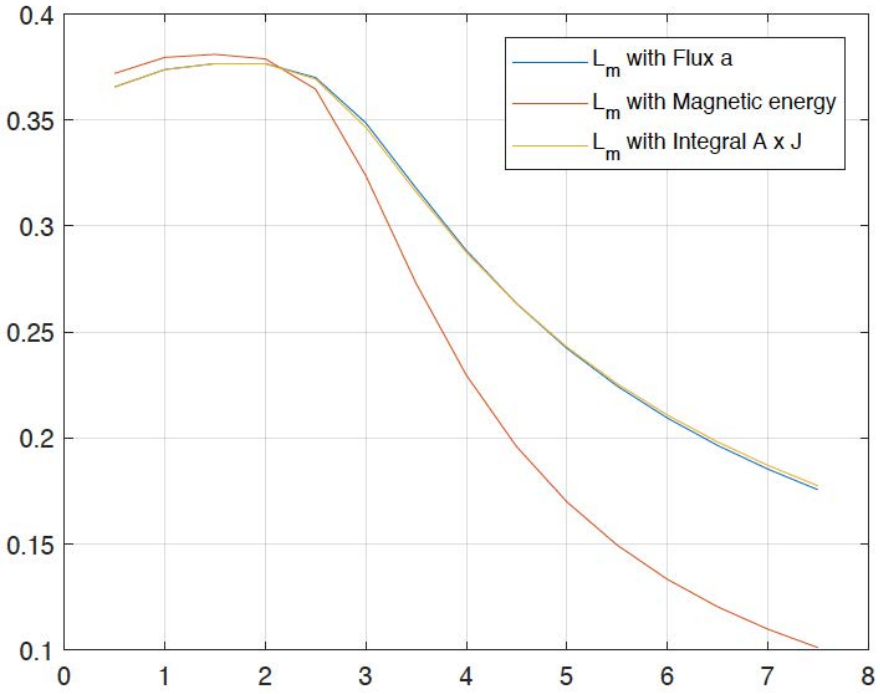

Figure 5.3 – Magnetize inductance [H] - current [A]

- With the integral of $\bar{A}_z \times \bar{J}$:

$$L_m = \frac{2\ W_{AJ}}{9\ \hat{I}^2} \tag{5.13}$$

where $W_{AJ} = W + W'$ can be calculated as:

$$W_{AJ} = \int_{vol} \bar{A}_z \times \bar{J}\ d\ Vol \tag{5.14}$$

With the value of magnetize inductance the total flux linkage can be calculated as :

$$\Lambda = L_m \cdot I_{rms} \tag{5.15}$$

And now, knowing the flux, the phase voltage of the machine can be computed:

$$V_{rms} = \omega \cdot \lambda \tag{5.16}$$

By doing the simulation from 0 to I_n the characteristic at no-load of the machine is obtained in where the saturation effect of the magnetic circuit is visible 5.4. From this characteristic, and knowing the phase voltage $E = 223.1\,\mathrm{V}$, it is possible to determine graphically the magnetize current of the machine $I_\mu = 2.75\,\mathrm{A}$.

$$\frac{I_s}{I_\mu} \simeq 50 \tag{5.17}$$

The ratio between the nominal phase current and the magnetize current is , according to the standard values for the induction machines [8]. Finally in 5.5 is reported the main harmonics of flux density at the airgap, it can be notice the effects of the presence of the slots. From the field solution, 5.2, by using the software F.E.M.M., it is possible verify in every point of the machine the values of the flux density.

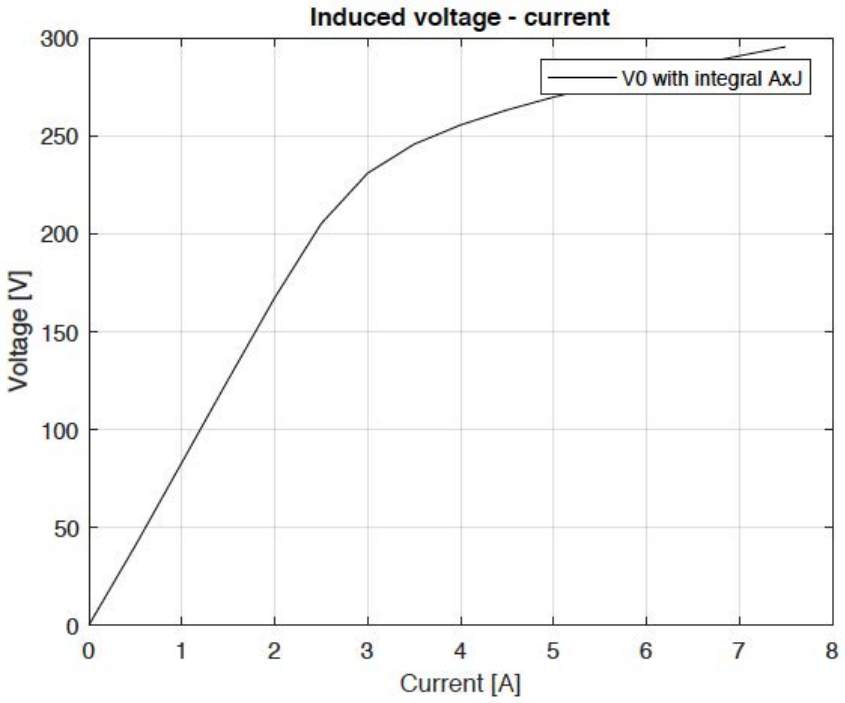

Figure 5.4 – No-load characteristic of the machine

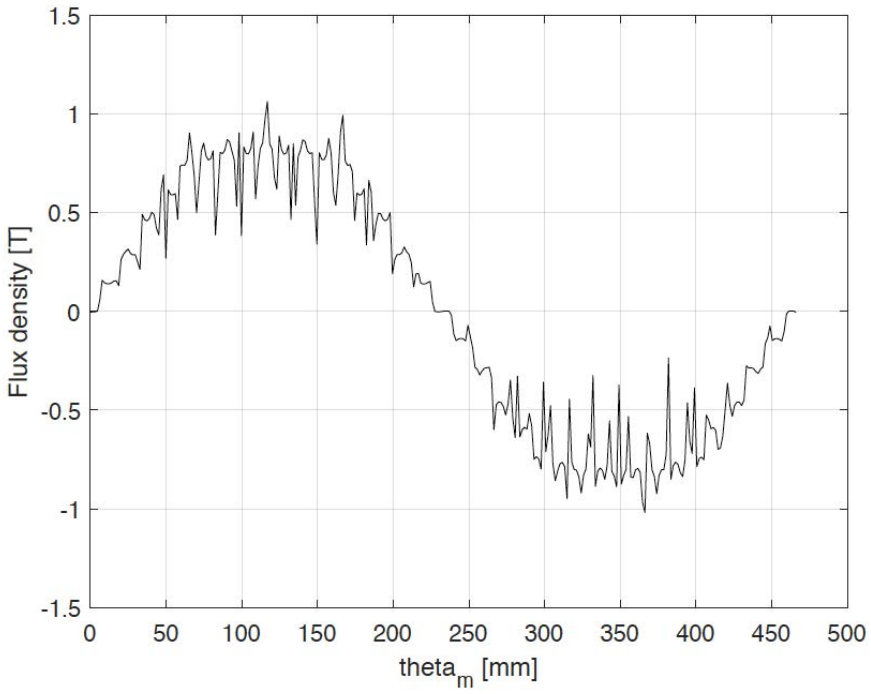

Figure 5.5 – Air gap flux density

5.2 Locked rotor simulation

By means of the locked-rotor test it can obtained the leakage inductance, $L_{\sigma\ 2D}$, and the rotor resistance, R_{r2D}, depending on the rotor frequency, i.e the relative values expressed with respect to the rotor. Since the rotor is locked, the rotor frequency coincides with the supply frequency, therefore various simulations will be performed, imposing stator currents with different frequency values. Before performing the simulation, some parameters of the machine model must be modified in the F.E.M.M. environment :

- the steel of the sheet of the machine is set linear (magnetic permeability $\mu_r = 4000$) because in this test the currents, imposed at the nominal value, corresponds to low voltage values therefore to a low values of magnetic flux as well.
- non-conductive and the copper of the windings.
- the electrical conductivity of aluminium of the rotor bars is maintained as the no-load simulation i.e. $\rho_{al} = 25\text{MS/m}$ at $120\,^{\circ}\text{C}$.

The electrical conduct aluminium of the rotor bars is The parameters of interest are obtained, as in the previous case without taking into account the 3D rotor effects, which will be added later. The motor is blocked in the position corresponding to the reference time t. The currents imposed are no longer constant, but sinusoidal:

$$i_a = \sqrt{2}\ I_s\,(\cos(0) + i\ \sin(0)) \tag{5.18}$$

$$i_b = \sqrt{2}\ I_s\left(\cos\left(-\frac{2\pi}{9}\right) + i\ \sin\left(-\frac{2\pi}{9}\right)\right) \tag{5.19}$$

$$i_c = \sqrt{2}\ I_s\left(\cos\left(-\frac{4\pi}{9}\right) + i\ \sin\left(-\frac{4\pi}{9}\right)\right) \tag{5.20}$$

$$i_d = \sqrt{2}\ I_s\left(\cos\left(-\frac{6\pi}{9}\right) + i\ \sin\left(-\frac{6\pi}{9}\right)\right) \tag{5.21}$$

$$i_e = \sqrt{2}\ I_s\left(\cos\left(-\frac{8\pi}{9}\right) + i\ \sin\left(-\frac{8\pi}{9}\right)\right) \tag{5.22}$$

$$i_f = \sqrt{2}\ I_s\left(\cos\left(-\frac{10\pi}{9}\right) + i\ \sin\left(-\frac{10\pi}{9}\right)\right) \tag{5.23}$$

$$i_g = \sqrt{2}\ I_s\left(\cos\left(-\frac{12\pi}{9}\right) + i\ \sin\left(-\frac{12\pi}{9}\right)\right) \tag{5.24}$$

$$i_h = \sqrt{2}\ I_s\left(\cos\left(-\frac{14\pi}{9}\right) + i\ \sin\left(-\frac{14\pi}{9}\right)\right) \tag{5.25}$$

$$i_i = \sqrt{2}\ I_s\left(\cos\left(-\frac{16\pi}{9}\right) + i\ \sin\left(-\frac{16\pi}{9}\right)\right) \tag{5.26}$$

By means of the finite element analysis the following data can be obtained:

- Magnetic energy W;
- Rotor joule losses P_{jr};
- Torque acting on the rotor by using Maxwell's stress tensor.

The field lines and the flux density map obtained can be viewed in the figures 5.6. It can be notice that at high frequency as in figure 5.6 the rotor has a shielding effect on the flux lines, indeed they are not able to enter in the rotor. The magnetic energy W and the rotor

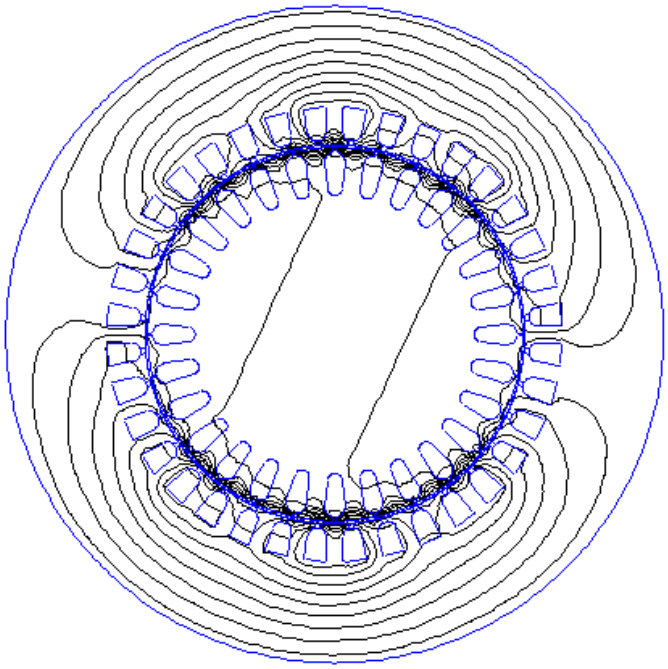

(a) *Flux line: blocked rotor test*

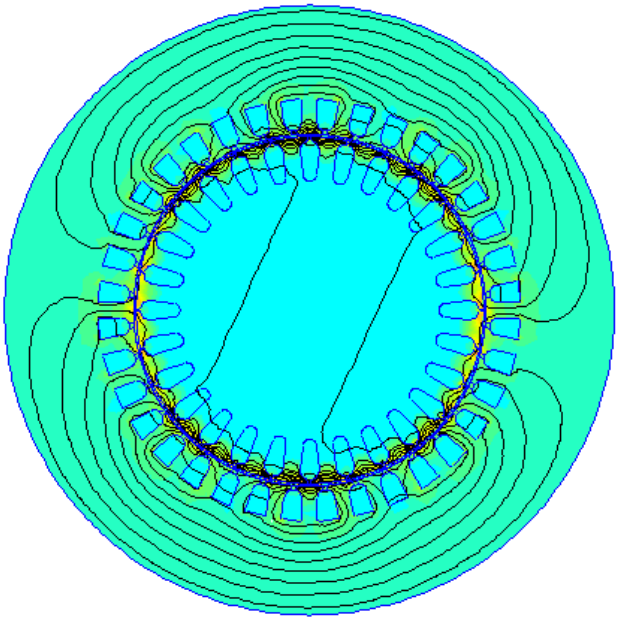

(b) *Flux density map*

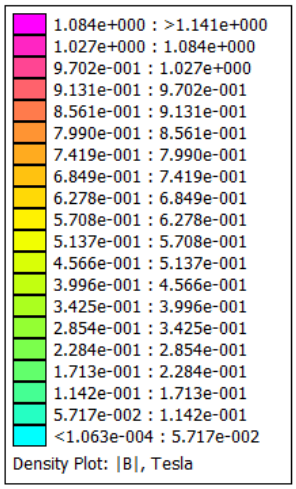

(c) *Legend*

Figure 5.6 – Blocked rotor test simulation

joule losses P_{jr} allow to calculate the resistive and inductive components of the impedance of the equivalent single-phase circuit which describes the rotor. The two part of the total impedance is calculate by:

$$R_{eq} = \frac{P_{jr}}{9 \cdot I_s^2} \tag{5.27}$$

$$L_{eq} = \frac{2 \cdot W}{9 \cdot I_s^2} \tag{5.28}$$

and they are reported in the figures 5.8 and 5.9 by varying the frequency. Then for obtain

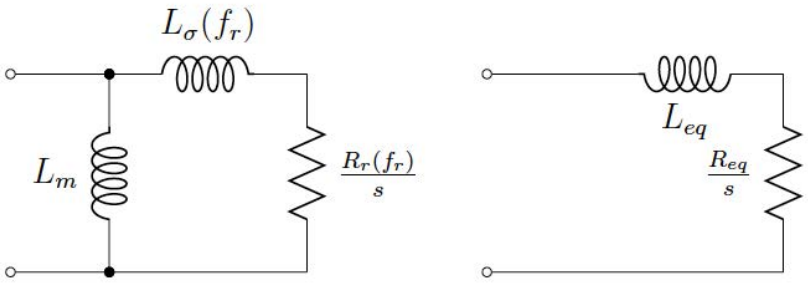

Figure 5.7 – Rotor equivalent circuit on Locked-rotor condition

the rotor parameters of the equivalent single-phase circuit of interest (first picture of 5.7), which is consisted in the parallel between the magnetization inductance and the series of rotor resistance and rotor leakage inductance, the equivalence between the 2 networks must be analyzed with 5.29 and 5.30:

$$L_{\sigma r}\ (f_r) = L_m \cdot \frac{L_{eq} \cdot (L_m - L_{eq}) - \dfrac{R_{eq}^2}{\omega^2}}{(L_m - L_{eq})^2 + \dfrac{R_{eq}^2}{\omega^2}} \tag{5.29}$$

$$R_r\ (f_r) = R_{eq} \cdot \frac{L_m + L_{\sigma r}}{L_m - L_{eq}} \tag{5.30}$$

where L_m is constant and is equal to the magnetize inductance calculated in these new conditions. The trend of the $L_{\sigma\ r}(f_r)$ and $Rr(fr)$ are reported in 5.11 and 5.10 by varying the frequency. It can be notice that in both plot, at low frequencies, there are a abnormal spike. This could be caused by numerical error during the process of the data in 5.29 and 5.30, and therefore only the main trend is consider for the next analysis. It is worth mentioning that the trend showing in 5.12 is not the true torque characteristic of the machine, but is the torque at nominal current calculated at several frequencies. By considering the nominal rotor frequency in this plot it will be possible to find the nominal torque. The torque acting to the rotor is calculated in two different ways:

- with the Maxwell's stress tensor directly from a F.E.M.M. tool,
- with the rotor joule losses from $T = P_{jr} \cdot p/(2\pi \cdot f)$

It can be notice that the two trends are very similar.

5.3 Performance

In order to calculate the performance of the machine by using the variable parameters equivalent circuit, it is necessary to add the parameters that take into account the three-dimensional effects of the final problem, effects which, as mentioned above, do not appear

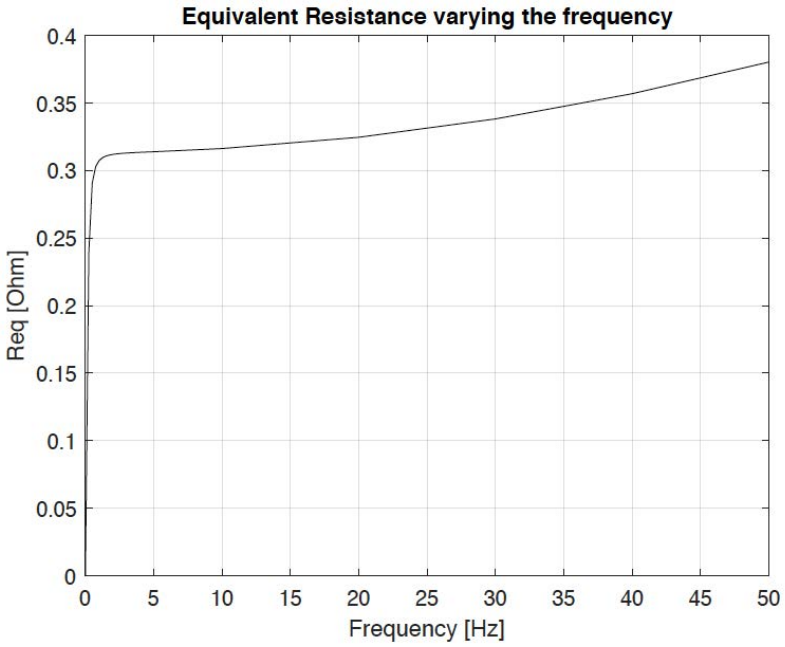

Figure 5.8 – Equivalent resistance

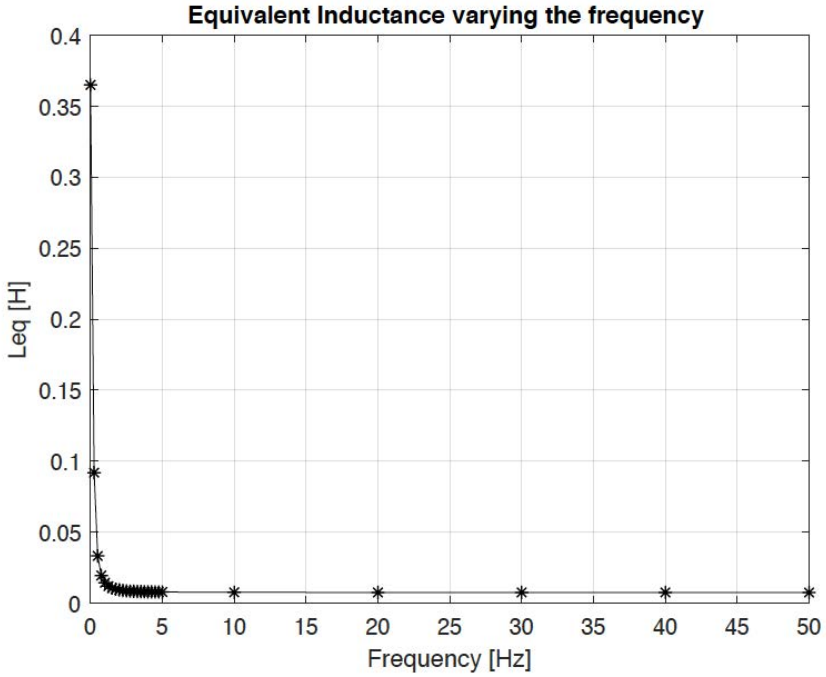

Figure 5.9 – Equivalent inductance

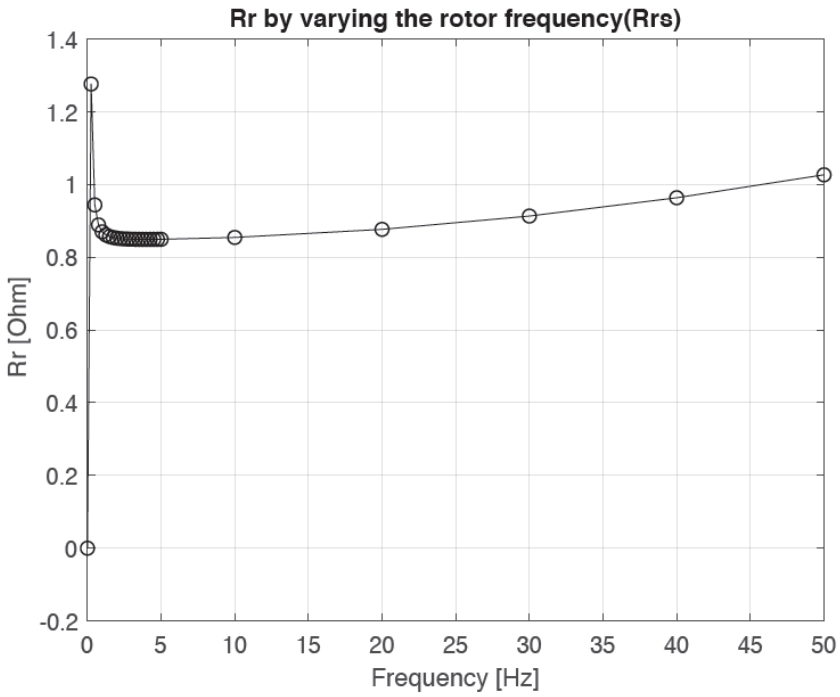

Figure 5.10 – Rotor resistance

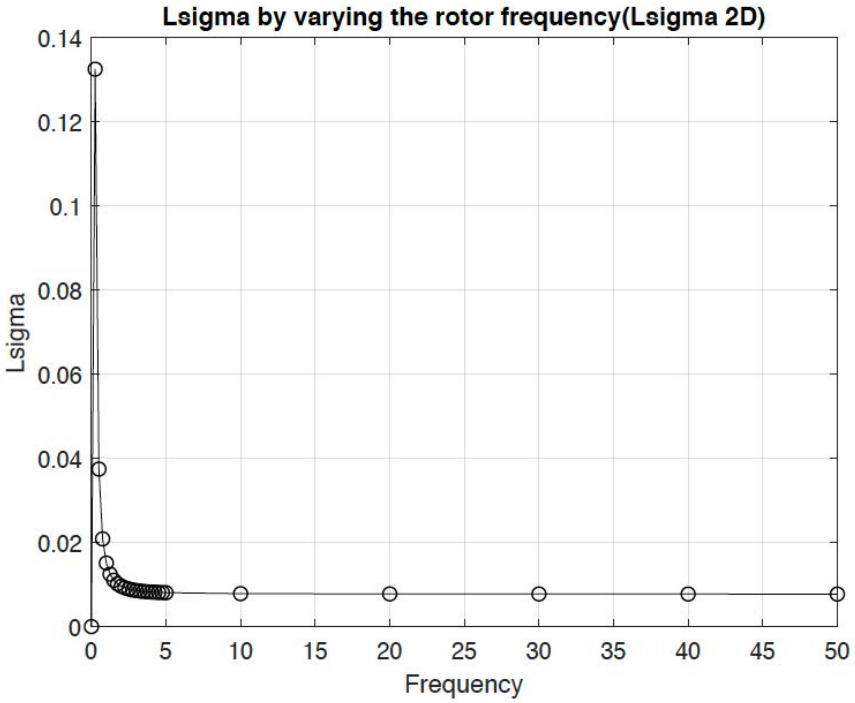

Figure 5.11 – Leakage rotor inductance

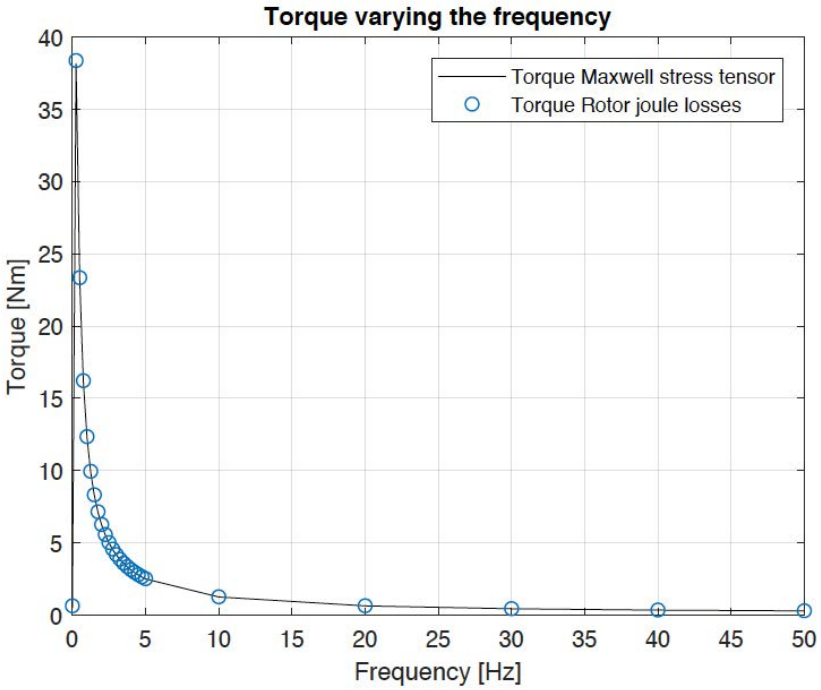

Figure 5.12 – Torque from Maxwell's stress tensor and From rotor losses

within the FEA simulations. These correction are analytical calculated. The rotor resistance must be corrected including the ring resistance, so in according to [3]:

$$K_{ring} = \frac{2\ Q_r\ D_r\ S_{bar}}{\pi\ 2p^2\ L\ S_{ring}} = 1.566 \tag{5.31}$$

where D_r and S_{ring} are the ring diameter and the ring cross section surface. Thus the resistance is corrected as:

$$R_r = R_{r\ 2D}\,(1 + K_{ring}) \tag{5.32}$$

The leakage inductance has to be corrected as well, with the effect of the end ring (5.33) and of the skewing.

$$L_{\sigma\ ring} = \mu_0\ k_r\ \frac{K_w}{K_{skew}}\ q^2\ \frac{\pi\ D_r}{L} = 0.00701\text{mA} \tag{5.33}$$

where $k_r = 0.36$ if $2p = 2$, $kr = 0.18$ if $2p > 2$, and k_w is the stator winding factor.

$$L_{\sigma\ tot} = L_{\sigma\ r} + L_{\sigma\ ring} + L_{\sigma\ skew} \tag{5.34}$$

By the construction of the equivalent circuit now it is possible to determine the performance of the machine. The mechanical characteristic of the machine is calculated, with the frequency-variant parameters obtained before, by using 5.35:

$$T_{em} = \frac{m\ p}{\omega}\ \frac{V^2}{\frac{R_s^2+X_\sigma^2}{R_r}\cdot s + 2R_s + \frac{R_r}{s}} \tag{5.35}$$

It can be notice that the maximum torque is very high with respect the classical values

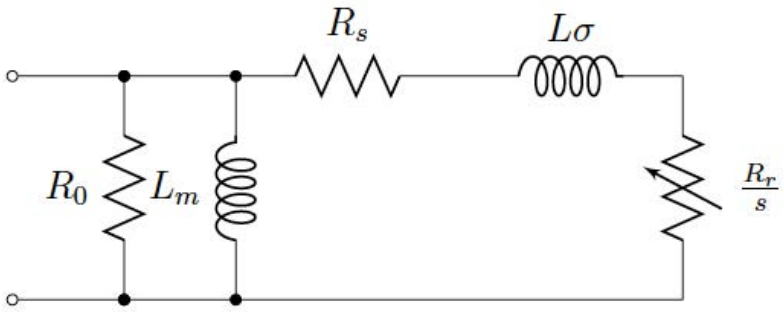

Figure 5.13 – Equivalent circuit of the machine

that can be found with a three-phase machine, but this is reasonable since the total leakage inductance of the machine is very low. Anyway, the field of work of a converter supplied machine is in the decreasing part of the characteristic. The nominal slip corresponding to the nominal torque $T = 30\,\mathrm{Nm}$ (blue line in 5.14) obtained from the simulation is $s = 0.016$. In figure 5.15 is reported the stator current density by varying the slip and in figure 5.16 is shown the power factor $\cos(\phi)$ by varying the slip; it can occur the estimation of the $\cos(\phi)$=0.9 in the fist part of the design 3 was acceptable. Finally the efficiency curve is reported in 5.17; is observable that the yield can reach high values, in particular the analytical prediction of $\eta = 88\%$ was correct for the nominal working point at $s = 0.016$. A big part of the total power losses of the machine derives from stator joule losses; this because the stator copper surface was design with the assumption of a current density $J_s = 5\,\mathrm{A/mm^2}$ which is a characteristic value in the design of three-phase IM [8]. Since in the multi-phase machine for the same power the current per phase is lower,it could be chosen a lower current density in order to increase the total copper surface and consequently to decrease the stator resistance. This could improve the total efficiency but with an increase of the quantity of the total copper.

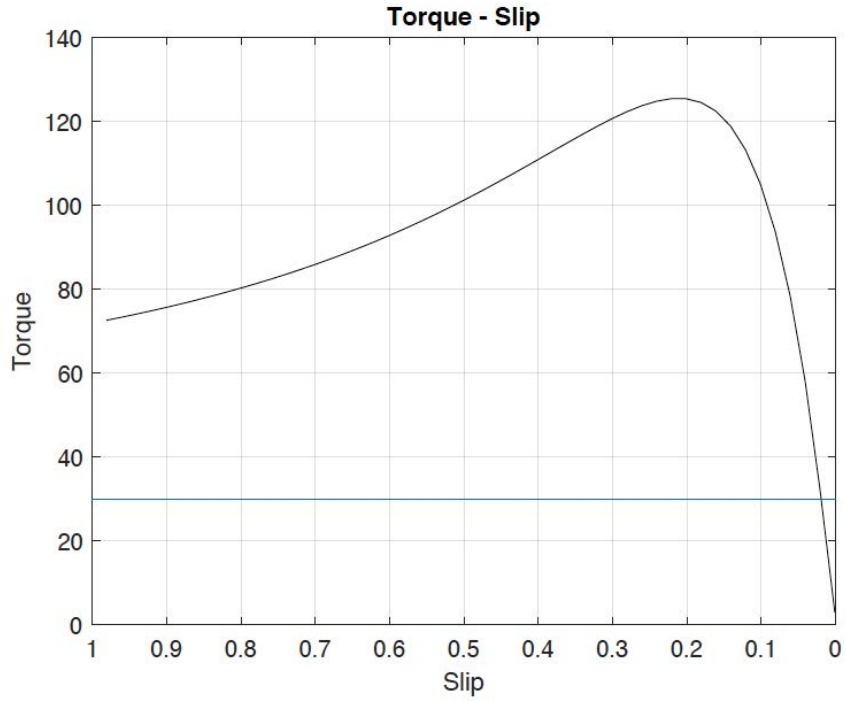

Figure 5.14 – Torque - slip characteristic

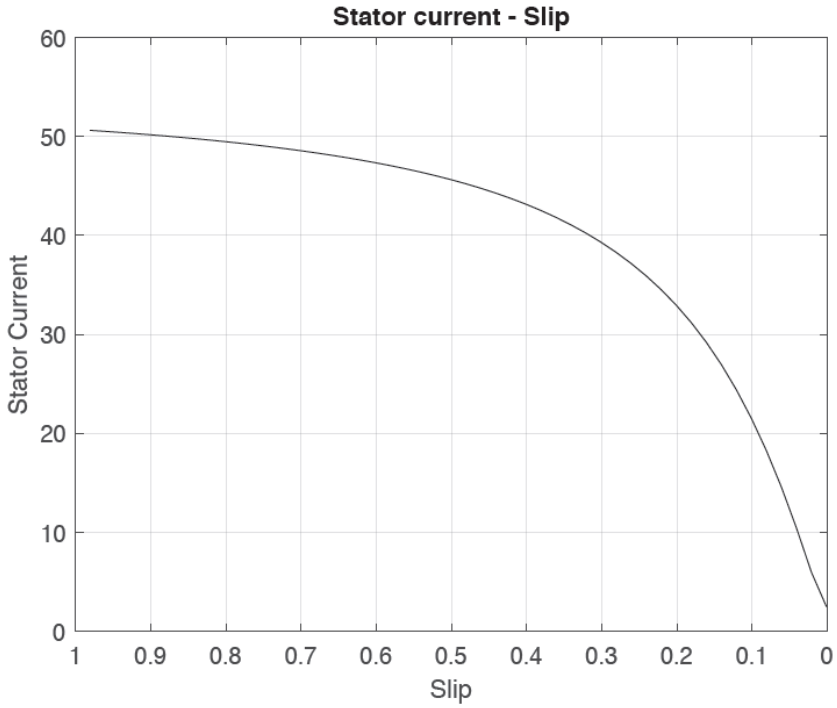

Figure 5.15 – Current slip characteristic

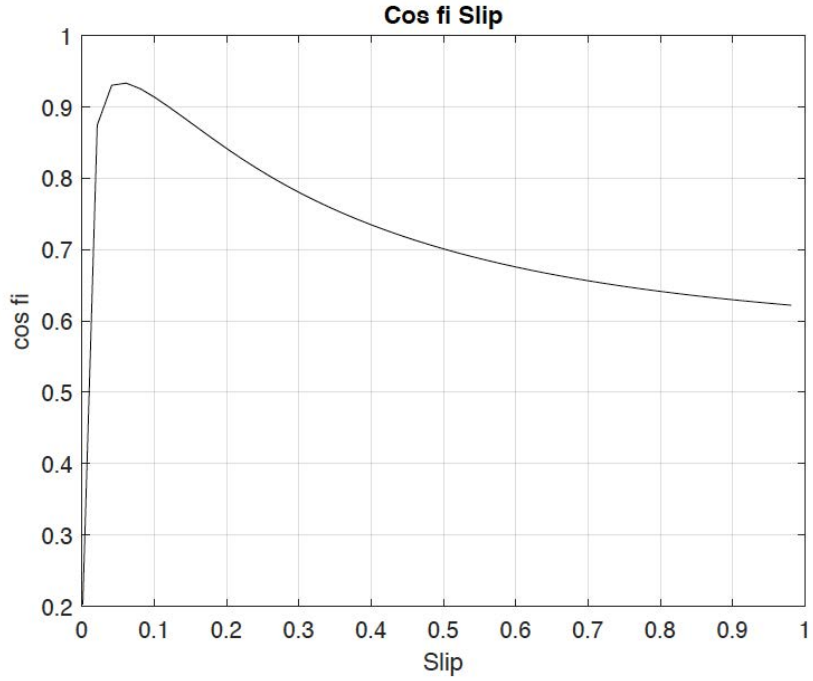

Figure 5.16 – Power factor

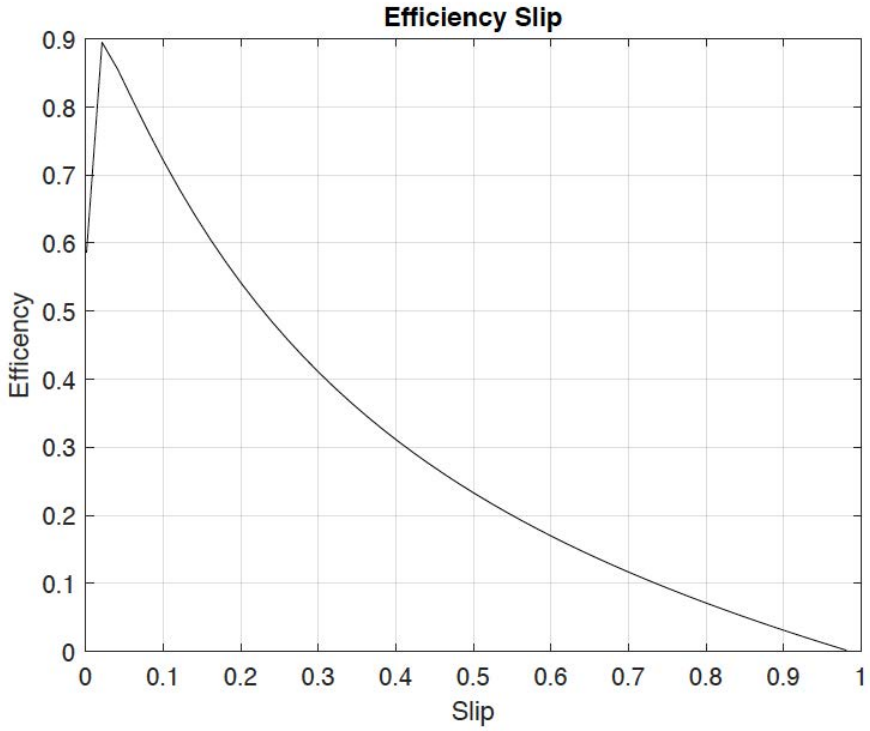

Figure 5.17 – Efficiency by varying the slip

6 Conclusions and further developments

The increasing of the interested in electrical mobility, has led to a rise in the studies regarding better and innovative solutions in the field of the electrical drive train like the multi-phase machine (m>3). The permanent magnet (PM) machines are largely adopted for these application due to their high power, high torque density and stator constructive ease. Nevertheless PM machines have drawbacks in sensitivity to heat and to inverse field, which can cause demagnetization, and in the cost of the rare-earth magnet which depends largely on markets led by few nation which have access. The induction machines (IM) can be an alternative interested solution to the PM machine. They are characterized by constructive ruggedness, rotor constructive ease and generally by a low manufacturing costs, but they have lower power density, since there is not the energy source from the magnets, and a sensitivity to the spatial harmonic content of the electrical quantities. This thesis work shows that IM can be that alternative because both the dimensions and the performance are comparable with the most designed PM found in scientific literature. In particular the reference machine for this work is the one designed in [22]. The results can be compared: the external and inner diameter of the PM machine are $D_{e\ pm} = 20$cm and $D_{pm} = 15.5$ cm instead for the IM designed in this work are $D_e = 26$ and $D = 15$ cm. Also the performance are very similar in the two cases with a torque $T_{pm} = 34.2$ Nm for the PM machine and a torque $T = 32$ Nm for the IM.

In designing of required IM, a general methodology is proposed, in particular for the synthesis of the stator winding. Induction machines work better with a distributed winding because it can ensure a near-sinusoidal MMF distribution which guarantees the best interaction between stator and rotor because the low harmonics content. Nevertheless designing a distributed winding becomes progressively more difficult as the number of phases increase. In chapter 2 all the issues related to the design of a multi-phase distributed winding are addressed and a general guide line is given. The most restrictive conditions are that the number of stator slots Q must be a multiple of the number of phase m, if a symmetrical distributed winding is desired, and the number of slot per pole per phase q must be greater than 1. It has been shown that a distributed winding with number of phase $m > 1$ is always possible but with a strong limitation in the possible choices of the set Q, q, $2p$. The final choice must be a compromise between the magnetic desired characteristics of the winding and its mechanical feasibility. The winding proposed for the machine is $Q = 36$, $q = 2$, $2p = 2$.

The finite elements analysis is performed by adopting the approach described in [7] and [3] that consist in combination between analytical and numerical results. The finite element simulation is bi-dimensional and all three-dimensional contribution are obtained with analytical procedure. This allows to save computational time, since the model is simplified, but also to have a good description of the iron saturation and the dependence of the rotor parameter by the rotor frequency. In order to do this two tests are simulate with the software: no-load test and blocked rotor test. The approaches shown in scientific literature are applied to the three-phase case. In this thesis the method is extend to nine-phase case and the results are

compared with analysis entirely performed in analytical way. The comparison shown that the results obtained with the two different ways are consistent, therefore this confirm that the approach, discussed in [7] and [3], is applicable also in a multi-phase case. Generally the performance with analytical and finite element model are similar and respects the design specification; a quick confirm is given by the trends of the two mechanical characteristics torque- slip calculated in the two ways: 4.3 and 5.14.

The possible further developments about the topic under investigation could be the construction of a Simulink model of the machine with the purpose of simulate the machine under the most common fault conditions. A description of these situation can be founded in [21]. The comparison with a design of a three-phase machine under the same nominal apparent power could be interest for understanding the differences from the classical case. Then the developing of a strategy of control that ensures the operation under fault condition in order to achieve an high level of reliability would be studied. Finally an optimization on the geometry founded in this work could be done in order to improve the performance, in particular the efficiency by optimizing the stator and rotor slots shapes and by choosing a higher number of poles with the aim to obtain a more compact machine.

Bibliography

[1] Alberti, L.: "Koil: A Tool to Design the Winding of Rotating Electric Machinery". In: *2018 XIII International Conference on Electrical Machines (ICEM)*. 2018.

[2] Alberti, L.; Bianchi, N.: "Design and tests on a fractional-slot induction machine". In: *2012 IEEE Energy Conversion Congress and Exposition (ECCE)*. IEEE. 2012.

[3] Alberti, L.; Bianchi, N.; Bolognani, S.: "A very rapid prediction of IM performance combining analytical and finite-element analysis". In: *IEEE Transactions on Industry Applications* (2008).

[4] Andriollo, M.; Martinelli, G.; Morini, A.: "Macchine elettriche rotanti". In: *Cortina editore* (2003).

[5] Barrero, F.; Duran, M. J.: "Recent advances in the design, modeling, and control of multiphase machines—Part I". In: *IEEE Transactions on Industrial Electronics* (2015).

[6] Bianchi, N.; Bolognani, S.; Comelato, G.: "Finite element analysis of three-phase induction motors: comparison of two different approaches". In: *IEEE Transactions on Energy Conversion* ().

[7] Bianchi, N.: *Electrical machine analysis using finite elements*. CRC press, 2005.

[8] Bianchi, N.; Bolognani, S.: *Metodologie di progettazione delle macchine elettriche*. Cleup, 2001.

[9] Boldea, I.; Nasar, S. A.: *The induction machine handbook*. CRC press, 2010.

[10] Dajaku, G.; Bilyi, V.; Gerling, D.: "Feasibility analysis of an improved FSCW for synchronous reluctance traction machines". In: *2017 IEEE International Electric Machines and Drives Conference (IEMDC)*. IEEE. 2017.

[11] JEKHA, V. R.: "Design of three phase induction motor by using Matlab". In: ().

[12] Kammermann, J.; Bolvashenkov, I.; Herzog, H.: "Improvement of Reliability and Fault Tolerance of Traction Drives by Means of Multiphase Actuators". In: 2017.

[13] Lekuona, J.: "Multiphase Machines and their Control in Healty and Faulty Mode". In: ().

[14] Levi, E.; Bojoi, R.; Profumo, F., et al.: "Multiphase induction motor drives–a technology status review". In: *IET Electric Power Applications* ().

[15] Levi, E.: "Multiphase electric machines for variable-speed applications". In: 2008.

[16] Meeker, D.: "Finite element method magnetics". In: *FEMM* (2010).

[17] Muller, G.; Vogt, K.; Ponick, B.: *Berechnung elektrischer maschinen*. John Wiley & Sons, 2008.

[18] Pyrhonen, J.; Jokinen, T.; Hrabovcova, V.: *Design of rotating electrical machines*. John Wiley & Sons, 2013.

[19] El-Refaie, A. M.; Shah, M. R.: “Comparison of Induction Machine Performance with Distributed and Fractional-Slot Concentrated Windings”. In: *2008 IEEE Industry Applications Society Annual Meeting*. 2008.

[20] Someda, G.: *Costruzione delle macchine elettriche*. Riccardo Patron, 1950.

[21] Souza, T. S. de; Bastos, R. R.; Cardoso Filho, B. J.: “Fault analysis in an inverter-fed nine-phase induction machine”. In: *2017 IEEE Energy Conversion Congress and Exposition (ECCE)*. IEEE. 2017.

[22] Tippe, L.; Kammermann, J.; Bolvashenkov, I., et al.: “Concept Analysis and Design of a 9-Phase Permanent Magnet Synchronous Machine”. In: *2018 AEIT International Annual Conference*. IEEE. 2018, pp. 1–6.